Static and Dynamic Contact Angle Measurement on Rough Surfaces Using Sessile Drop Profile Analysis with Application to Water Management in Low Temperature Fuel Cells

By

Vinaykumar Konduru

A THESIS

Submitted in partial fulfillment of the requirements for the degree of

MASTER OF SCIENCE

(Mechanical Engineering)

MICHIGAN TECHNOLOGICAL UNIVERSITY

2010

This thesis, "Static and Dynamic Contact Angle Measurement on Rough Surfaces Using Sessile Drop Profile Analysis with Application to Water Management in Low Temperature Fuel Cells," is hereby approved in partial fulfillment for the requirements for the Degree of MASTER OF SCIENCE IN Mechanical Engineering.

Department of Mechanical Engineering – Engineering Mechanics

Advisor:	______________________
	Dr. Jeffrey S. Allen
Committee Member:	______________________
	Dr. Jaroslaw Drelich
Committee Member:	______________________
	Dr. Chang Kyoung Choi
Department Chair:	______________________
	Professor William W. Predebon
Date:	______________________

Abstract

Fuel Cells are a promising alternative energy technology. One of the biggest problems that exists in fuel cell is that of water management. A better understanding of wettability characteristics in the fuel cells is needed to alleviate the problem of water management. Contact angle data on gas diffusion layers (GDL) of the fuel cells can be used to characterize the wettability of GDL in fuel cells. A contact angle measurement program has been developed to measure the contact angle of sessile drops from drop images. Digitization of drop images induces pixel errors in the contact angle measurement process. The resulting uncertainty in contact angle measurement has been analyzed. An experimental apparatus has been developed for contact angle measurements at different temperature, with the feature to measure advancing and receding contact angles on gas diffusion layers of fuel cells.

Acknowledgments

I owe my deepest gratitude to my advisor Dr. Jeffrey Allen for whose continuous support, patience and guidance enabled me in all time of research and writing this thesis. I would also like to thank the entire MNiT research group and Chelsey Smith in particular for the help she provided in collecting the data for my work.

Contents

List of Figures

List of Tables

Chapter 1. Introduction

In a proton exchange membrane (PEM) fuel cell, hydrogen and oxygen react to form electricity, water and heat. The basic assembly of a PEM fuel cell consists of polymer electrolyte membrane which is sandwiched between two electrodes. These electrodes which are called gas diffusion layers (GDL) are made up of carbon cloth or carbon paper. A catalyst layer is bonded to the polymer membrane. This catalyst layer helps in accelerating the rate of reactions. The GDL is coated with poly(tetrafluoroethylene) (PTFE) to make the surface hydrophobic. This aides in the removal of water to the surface of GDL. Such an arrangement of GDLs with a polymer electrolyte membrane with catalyst forms a single fuel cell and is commonly called as membrane electrode assembly (MEA). Different cells are connected together by means of bipolar plates. The bipolar plates have channels built into them that carry the reactants to the fuel cell and also collect the water produced in the fuel cell (Figure 1.1).

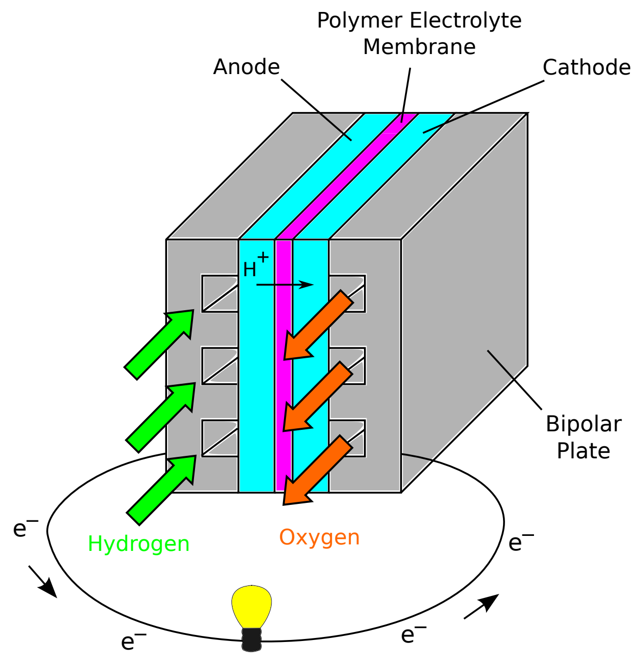

Figure 1.1. PEM Fuel Cell Assembly

During operation, hydrogen in passed over anode and oxygen over cathode. At anode, hydrogen gas dissociates producing protons and electrons. Protons travel through the electrolyte membrane while electrons travel through the circuit. At cathode, they react with oxygen to form water. These reactions are given in Equations (1.1)-(1.3).

$$\text{At Anode: } \; H_2 = 2H^+ + 2e^- \tag{1.1}$$

$$\text{At Cathode: } O_2 + 4H^+ + 4e^- = 2H_2O \tag{1.2}$$

$$\text{Net cell Reaction: } 2H_2 + O_2 = 2H_2O \tag{1.3}$$

Water management in a fuel cell plays a vital role for the optimal performance of a fuel cell. Water that is formed at cathode during the fuel cell operation is removed by the reactant flow. The membrane is kept hydrated as the proton conductivity increases with water content. If excess water is withdrawn, the membrane will dry out and thereby increasing the resistance to the motion of protons reducing the fuel cell performance. If the water removal rate is slow, the excess water that is produced forms plugs in the channels and thereby blocking the path of reactant gases and reducing the number of available reaction sites severely hampering fuel cell operation [Larminie and Dicks, 2003].

To solve the problem of water management, an understanding of wetting characteristics of GDLs is essential. One way to characterize the GDLs is by virtue of analyzing the contact angle it makes with water. The contact angle is defined as the angle made by the liquid in contact with solid surface and measured from the liquid side (Figure 1.2). The static contact angle between a liquid drop and a smooth solid surface is given but the Young's Equation (1.4) which essentially is the force balance between the interfacial tensions at the solid-liquid-vapor interface.

$$\sigma_{LV} \cos(\theta) = \sigma_{SV} - \sigma_{SL} \tag{1.4}$$

In the fuel cell, dynamic conditions exist. Water drops that are formed on the GDL move over the GDL in the channels and for this reason dynamic contact angle needs to be measured.

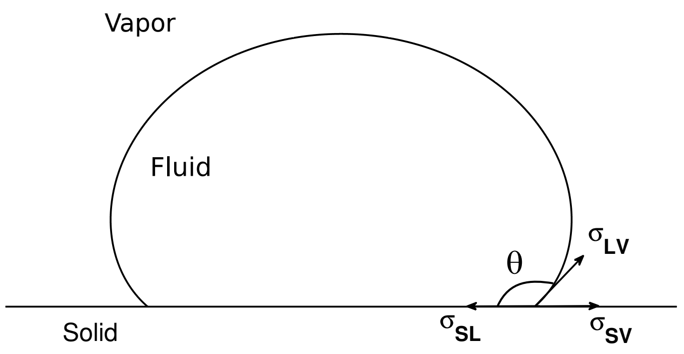

Figure 1.2. Young's Model of Sessile Drop showing relationship between Interfacial Tensions

1.1 Techniques for Measuring Contact Angle

Several techniques exist to determine the contact angle, principal among them being the Wilhelmy Plate method and goniometry.

1.1.1 Wilhelmy Plate Method

This technique can be used to measure the contact angle if the surface tension of the liquid is known. Similarly, if the contact angle for the given solid-liquid pair is known, surface tension of the liquid can be obtained with this method. Wilhelmy plate method essentially consists of a rectangular plate on which angle is to be measured and a reservoir of the fluid kept below the plate. To measure the contact angle, the fluid is raised towards the plate until it touches the plate (Figure 1.3). The change in the weight of the plate (ΔW) occurs because of the liquid adhering to the plate. This change in weight is measured and with the knowledge of the wetted perimeter (p), the contact angle (θ) is measured from Equation 1.5.

$$\sigma \cos(\theta) = \frac{\Delta W}{p} \tag{1.5}$$

This method of measuring the contact angle is not suitable for rough and porous substrates such as GDLs. The fibrous surface of a GDL coupled with pores makes it difficult to measure the perimeter and may also result in wicking of the fluid into the GDL which result in incorrect weight measurements producing incorrect contact angle results. A modification of the Wilhelmy plate method is the Single Fiber Wilhelmy method in which the plate is replaced by a single fiber of the substrate. The single fiber however is not an accurate representation of the actual GDL surface.

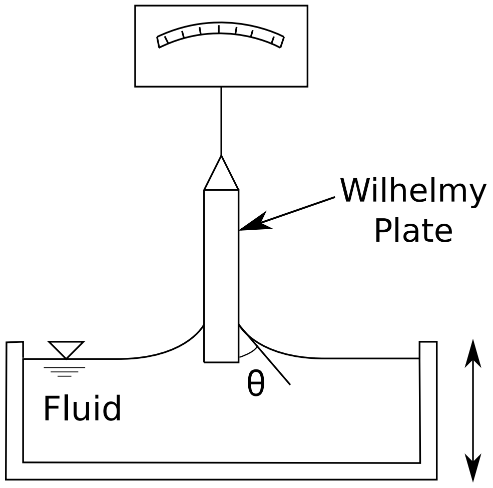

Figure 1.3. Contact angle measurement using Wilhelmy Plate method

1.1.2 Goniometry

In goniometry, an image of the drop is obtained and contact angle is measured from the drop image. An elementary method is to draw a tangent and the solid-liquid interface along the drop profile and measure the contact angle. This method is very crude and the obtained angle is dependent on the judgement of the user and hence this method is not suitable for scientific applications.

For very small drops with Bond number (Bo) less than 1, spherical cap approximation can be applied in which the drop shape is approximated to that of a sphere by neglecting the effects of gravity. This approximation fails if the Bond number becomes greater than 1 as the effects of gravity cannot be neglected. The small slope approach [Allen, 2003] presents a simple model to obtain contact angles which are less than 30° but can be applied to drops of any size.

$$\left(\frac{1}{R_1}+\frac{1}{R_2}\right)\sigma=\Delta P \tag{1.6}$$

Contact angle measurement by fitting a curve to the drop edge gets rid of the size constraints imposed by previous methods. Multiple points on the drop edge are selected from the images and a B-spline [Stalder et al., 2006] or any other curve is fitted to these profile points. Another approach is to model the drops using the Laplace-Young equation (1.6). A numerical solution to this equation was first developed by Bashforth and Adams [1883]. Hartland and Hartley [1976] solved the Laplace-Young equation numerically using the fourth order Runge-Kutta method and obtained the exact drop profile for different drop parameters. Cheng et al. [1990] followed a similar approach and developed a technique called Axisymmetric Drop Shape Analysis (ADSA), to fit the obtained theoretical drop profiles to the drop edge obtained from the images.

Young's equation (1.4) is applicable to systems with smooth and homogeneous surfaces only. On rough and heterogenous surfaces as found on GDLs, contact angles obtained using Young's correlation would be incorrect. Modifications to the Young's equation have been established previously and will be discussed in Section 1.2

1.2 Contact Angle on Rough Surfaces

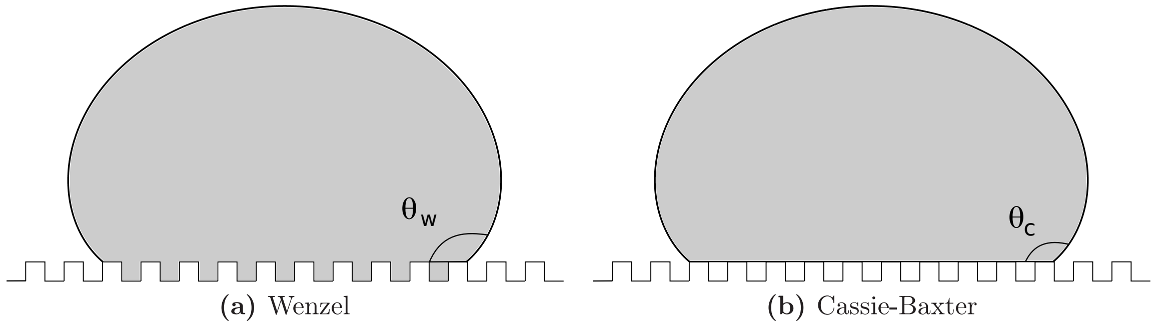

(a) Wenzel **(b)** Cassie-Baxter

Figure 1.4. Wetting on Rough Surfaces

A drop of liquid on a rough surface can take either of the two forms *a*) Total wetting (Figure 1.4a), where the liquid wets the entire rough surface; or *b*) Partial wetting (Figure 1.4b), where vapor is trapped between the liquid and the troughs of the rough surface. For the case of total wetting, Wenzel [1936] developed Equation 1.7 to model the apparent contact angle (θ_W) on rough surfaces. Roughness factor (r) is the ratio of the true surface area and the projected surface area. For non-wetting surfaces ($\theta > 90°$), an increase in roughness would increase the apparent contact angle and for wetting surfaces ($\theta < 90°$), increased surface roughness woud reduce the apparent contact angle.

$$\cos(\theta_W) = r\cos(\theta_Y) \tag{1.7}$$

Cassie and Baxter [1944] developed Equation 1.8 to model contact angle on heterogenous surfaces, where f_i is the fraction area of each surface under the liquid and θ_{Y_i} is the contact angle for the same surface. For the case of partial wetting with vapor trapped between the solid and liquid, 1.8 takes the form of Equation 1.9, where f_1 is the fractional area for the solid-liquid interface and f_2 is the fractional area for the pores.

$$\cos(\theta_C) = \sum f_i \cos(\theta_{Y_i}) \tag{1.8}$$

$$\cos(\theta_C) = f_1 \cos(\theta_Y) - f_2 \tag{1.9}$$

The Wenzel 1.7 and Cassie-Baxter 1.9 do not consider the irregularities that occur at the solid-liquid-vapor contact line. Several modifications to these equations have been published. Drelich and Miller [1993], have suggested modifications to the above equations for different configurations of the surface at the contact line. However, due to the lack of a uniform surface on a GDL, these equations are not applicable on GDLs.

Chapter 2. Sessile Drop Profile Analysis

The Laplace equation of capillarity is the mathematical balance between the surface tension forces and gravitational forces, for two fluids separated by an interface.

$$\left(\frac{1}{R_1}+\frac{1}{R_2}\right)\sigma=\Delta P \tag{2.1}$$

where σ is the interfacial tension, $\Delta\ P$ is the pressure difference across the interface, R_1 and R_2 are the two principal radii at the apex. The pressure difference consists of two components, the hydrostatic pressure (P_g) and the pressure due to the curvature (P_σ). These are expressed as

$$\Delta P_g=\rho g z \tag{2.2}$$

$$\Delta P_\sigma=\frac{2\sigma}{b} \tag{2.3}$$

Thus for any sessile drop, at a height of z from apex, the Laplace equation can be expressed as

$$\left(\frac{1}{R_1}+\frac{1}{R_2}\right)\sigma=\frac{2\sigma}{b}+\rho g z \tag{2.4}$$

At apex of the drop, due to symmetry of an axisymmetric drop, $R_1=R_2=b$ where b is the radius of curvature at the apex. The two radii of curvature can be expressed in terms of the arc length and the angle of the tangent to the interface by recognizing that

$$\frac{1}{R_1}=\frac{d\theta}{ds} \tag{2.5}$$

$$\frac{1}{R_2}=\frac{\sin(\theta)}{x} \tag{2.6}$$

Equation (2.4) is then expressed as

$$\frac{d\theta}{ds} = \frac{2}{b} + \frac{\rho g z}{\sigma} - \frac{\sin(\theta)}{x} \tag{2.7}$$

To solve equation (2.7), it is non-dimensionalized using the capillary constant, c, which is the ratio of physical properties of the fluid, namely the density, surface tension and gravity and has the dimensions of 1/length^2.

$$c = \frac{\rho g}{\sigma} \tag{2.8}$$

The non-dimensionalized parameters that are needed to define the drop profile are

$$X = xc^{\frac{1}{2}} \tag{2.9}$$

$$Z = zc^{\frac{1}{2}} \tag{2.10}$$

$$B = bc^{\frac{1}{2}} \tag{2.11}$$

$$S = sc^{\frac{1}{2}} \tag{2.12}$$

In non-dimensionalized form, equation (2.7) is expressed as

$$\frac{d\theta}{dS} = \frac{2}{B} + Z - \frac{\sin(\theta)}{X} \tag{2.13}$$

Equation (2.13) with the geometric definitions, equations (2.14) and (2.15) form a set of first order differential equations which are solved numerically to obtain the required drop profile.

$$\frac{dX}{dS} = \cos(\theta) \tag{2.14}$$

$$\frac{dZ}{dS} = \sin(\theta) \tag{2.15}$$

In order to solve the above set of equations, different solvers exist in MATLAB®. The `ode45` solver, which utlizes the Runge-Kutta method, was selected to obtain the drop profile. To validate the obtained profile, a comparison is made between the profile obtained from `ode45` and the numerical data published by Hartland and Hartley [1976]. Data points at $\theta = 90°$ are selected for comparision (Table 2.1). The obtained profile points are accurate and deviate only in the fourth digit, which enables us to conclude that an accurate drop profile is generated.

Table 2.1. Comparision of data points with numerical data published by Hartland and Hartley [1976]

B	Hartland and Hartley		ODE45	
	X90	Z90	X90	Z90
-1.50	.0316175	.0316102	0.031627	0.031658
-1.25	.0562045	.0561636	0.056224	0.056221
-1.00	.0998342	.0996054	0.099872	0.099588
-0.75	.176906	.175646	0.176973	0.175620
-0.50	.311216	.304568	0.311345	0.304596
-0.25	.536715	.505309	0.537020	0.505450
0.00	.885291	.766710	0.885116	0.766908
0.25	1.35895	1.02957	1.359368	1.029598
0.50	1.92291	1.23563	1.923322	1.235702
0.75	2.53445	1.370590	2.534496	1.370668
1.00	3.16457	1.44869	3.164281	1.448872

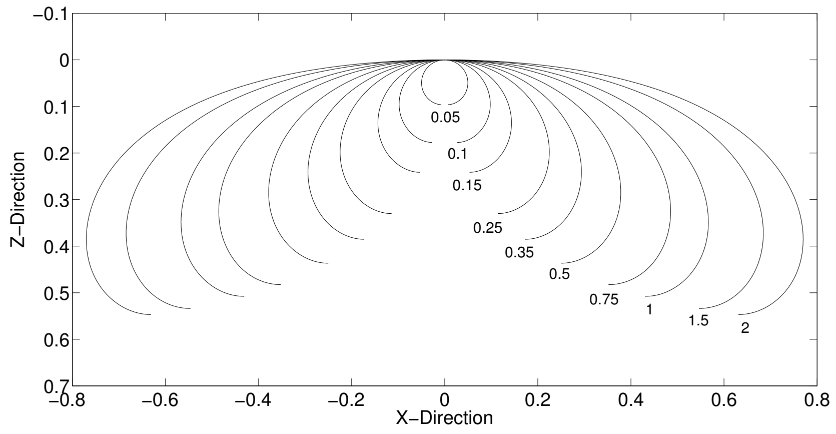

Figure 2.1. Variation in drop shape with respect to dimensionless radius of curvature at apex, *B*

To generate a drop profile in non-dimensional co-ordinates, value of only the dependent variable B is needed. Figure 2.1 shows the drop profiles that are obtained for different values of B. The drop profiles are dimensionalised by dividing them with $c^{1/2}$. The capillary constant thus acts as a scaling factor for the generated drop profiles. Figure 2.2 shows drops generated with same B but at different values of capillary constant.

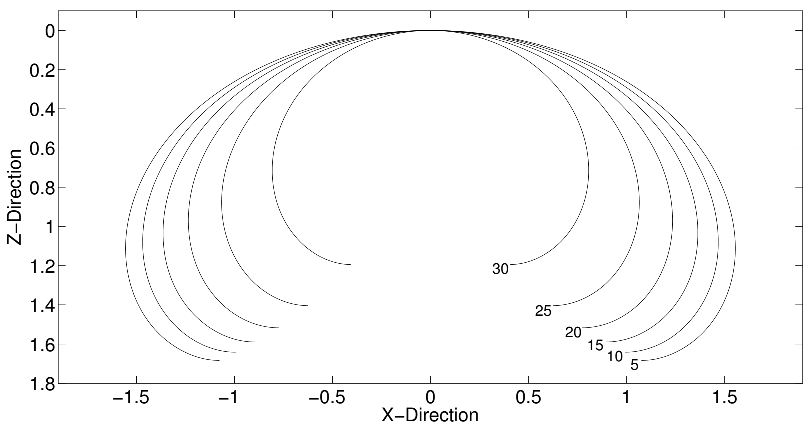

Figure 2.2. Variation in drop shape with respect to c (cm^{-2}) at constant $B = 0.4$

2.1 Numerical Optimization

The error between the Laplacian curve and the drop profile is defined as the sum of the normal distance between the drop profile and the Laplacian curve. By applying suitable edge detection techniques described in Section 3.1 the drop edge is obtained. On this edge, co-ordinates of N number of points are obtained (Figure 2.3). To calculate the error between the Laplacian curve and the actual profile, a normal is drawn from the N points onto the estimated Laplacian curve. The length of the normal gives the magnitude of error at that point. The total error is the sum of magnitude of distances calculated for all points. The distance is positive if the data point on the drop lies on one side of the the Laplacian curve and negative if it lies on the other side.

If B is kept constant and only fluid properties are changed by varying c, the error obtained for a given drop is minimum only for one value of c. This c would then be the optimal capillary constant corresponding to that value of B. The error obtained for this B-c pair would be the absolute minimum error that exists for B. Thus for different values of B, the error is obtained and the one that yields minimum error gives the solution from which contact angle is determined. Following is the procedure that is utilized to obtain accurate drop profiles:

1. Guess the initial value of B, which is close to the actual value. The program `Initial guess` performs this function and utilizes the algorithm developed by Stacey [2009].

2. Five values of B, two on each side of the initial guess, are selected. Obtain

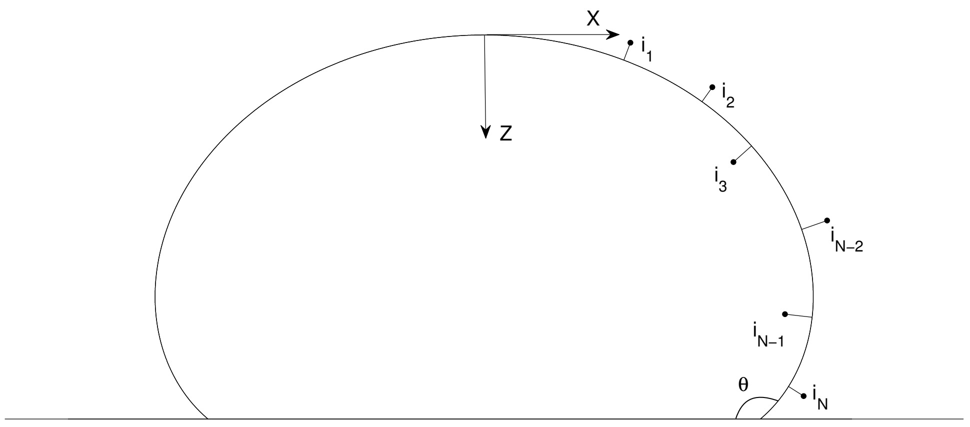

Figure 2.3. Calculation of error over the drop profile. (offsets are exagerrated)

the capillary constant for each that results in minimum error by employing the bisection method (Figure 2.4).

3. Out of these five, the value that yields minimum error and adjacent two values

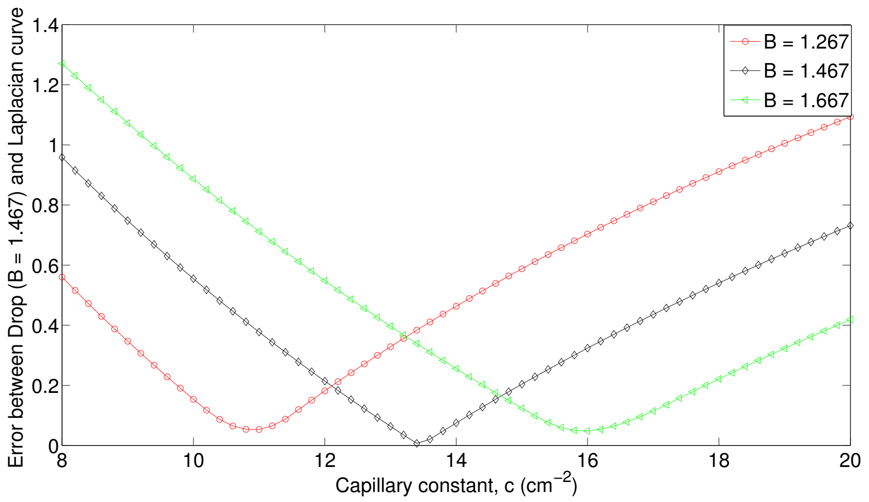

Figure 2.4. Variation of error vs capillary constant at same non-dimensionalized radius of curvature at apex, B. Actual drop $B = 1.467$, $c = 13.45$ (cm^{-2})

are retained and the other two values are discarded. The span between the remaining three values is divided equally to obtain 2 more values of B where the error is calculated again. This procedure is repeated till the limit of error in B is within $\pm 5e^{-5}$ (Figure 2.5 and 2.6). Typically 10 iterations are required to achieve this accuracy.

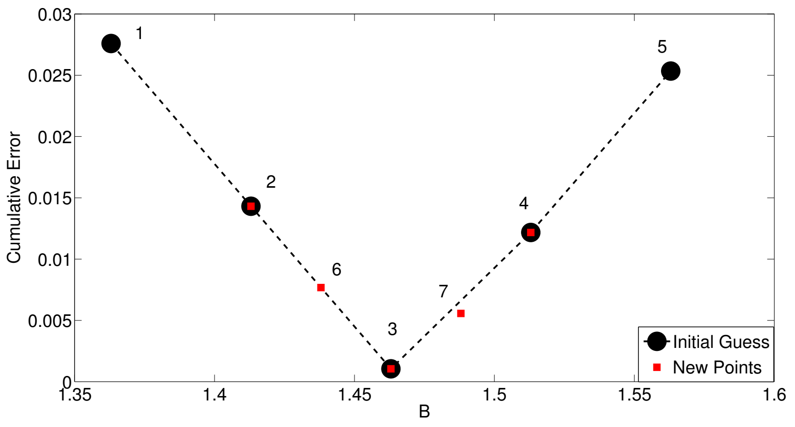

Figure 2.5. Error optimization (First iteration). (True $B = 1.467$, $c = 13.45\ cm^{-2}$) Points 1-5: Error at initial values of B. Points 1 and 5: Discarded after step 1. Points 6 and 7: New guessed values.

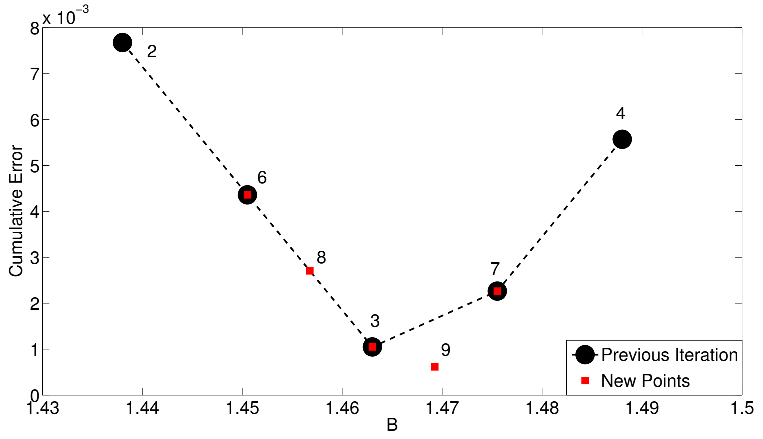

Figure 2.6. Error optimization (Second iteration). (True $B = 1.467$, $c = 13.45\ cm^{-2}$) Points 2 and 4: Discarded after step 2. Points 8 and 9: New guessed values.

Figure 2.5 shows the results from the first iteration. Circles (points 1-5) represent the initially guessed values while the squares (points 6-7) represent the new values for the next iteration. (Figure 2.6) shows the results from second iteration. Circles represent data from previous iteration while the squares represent new data points. Comparing the two figures, it is seen that the error in the drop profile reduces for each iteration.

2.2 Code Verification

To test the accuracy with which the code determines the contact angle, a drop profile was generated using the Laplace-Young equation. Twenty one points selected from this profile and the co-ordinates of these points were supplied to the program. The program can be said to operate accurately if the obtained values of b, c and the contact angle are the same as those that were used to generate the profile. Cheng et al. [1990] discusses the effect of the number of points used for edge detection on the resultant contact angle. Significant improvement in accuracy was not seen when more points were selected. Table 2.2 shows the obtained values of b and c and the actual values. Also the corresponding theta that is obtained from the program is shown. The test validates that for a given drop profile the program yields an accurate contact angle. It also shows that twenty one points are sufficent for contact angle calculation. However, selection of more points would result in a better estimation of the drop edge [Neumann and Spelt, 1996] at the expense of computational time.

Table 2.2. Code Verification for $\theta = 160\,^{\circ}$; c = 13.45 cm^{-2}

Actual	Obtained		
b	c	b	θ
0.15	13.4506	0.1500	159.94
0.20	13.4502	0.2000	159.99
0.25	13.4497	0.2500	159.98
0.30	13.4504	0.3000	159.99
0.35	13.4501	0.3500	159.99
0.40	13.4500	0.4000	160.00
0.45	13.4497	0.4500	159.99
0.50	13.4502	0.5000	159.99
0.75	13.4501	0.7500	159.99
1.00	13.4499	1.0000	159.99
1.50	13.4500	1.5000	159.99
2.00	13.4500	2.0000	159.99

Chapter 3. Accuracy in Contact Angle Measurement

The accuracy in contact angle measurement depends upon the image processing technique that is applied for extracting the drop edge from the sessile drop images. This chapter explains in details the effect of inaccuracies in edge detection on contact angle measurement.

3.1 Drop edge detection

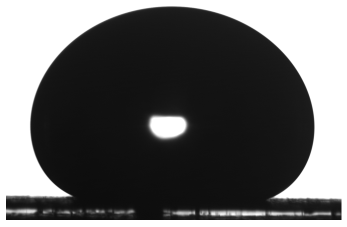

(a) Sessile Drop

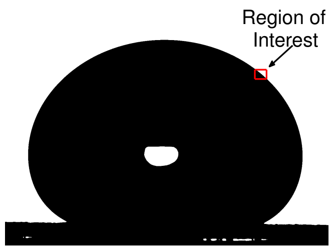

(b) Gray-scale Image

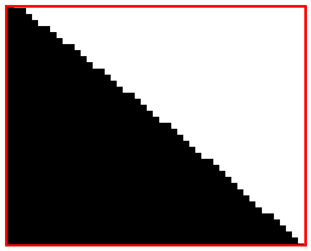

(c) Pixelation in Gray-Scale Image

Figure 3.1. Drop Edge Detection (GDL: Toray T060,9%PTFE(wt))

The drop image (Figure 3.1a) is converted into a gray-scale image (Figure 3.1b) by thresholding. The gray-scale image consists of a dark foreground representing the drop and a white background. The edge of the drop, however, is not accurate as it consists of step changes in the profile (Figure 3.1c). An actual drop profile is expected to be smooth and continuous. In addition, the obtained profile would depend on the value set for thresholding. To obtain the accurate drop edge [Cheng et al., 1990], intensities of pixels along a normal across the drop edge are found (Figure 3.2). The pixel intensities for 11 pixels along with a cubic spline fit is shown in Figure 3.3. From the figure, we see a sharp drop in pixel intensity as we move from the background into the drop. The edge of the drop is expected to be in a region along the spline where the gradient is high. From Figure 3.3, it is evident that there lies an uncertainty in exact edge detection and the edge is therefore approximated to lie in the region of 2-3 pixels along the normal. The effect of this uncertainty on contact angle measurements in explained in detail in Section 3.2. This procedure of finding the edge along the normal is repeated over the entire drop profile. To further increase the accuracy by eliminating the step changes that occur at the edge, a second-order least square polynomial is fitted to 11 adjacent points along the edge, and the drop edge is obtained from these polynomials.

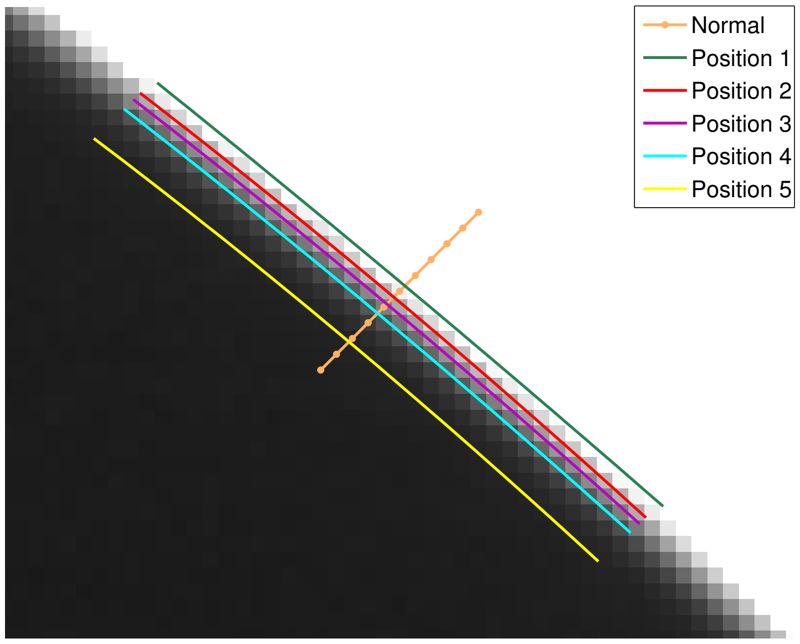

Figure 3.2. Edge Detection Approximation

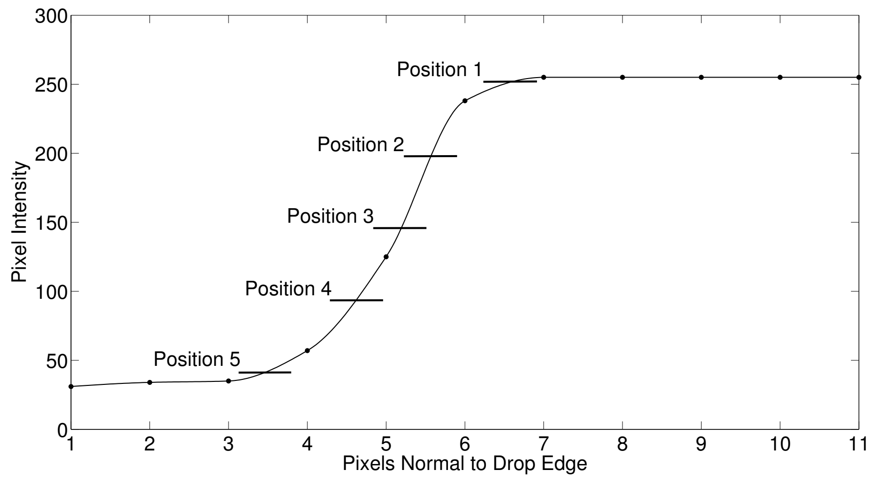

Figure 3.3. Change in pixel intensity along normal to drop profile. Pixel intensities for Figure 3.2.

3.2 Edge Detection Accuracy

The uncertainty that exists in drop edge detection causes the obtained contact angles to become a function of the methodology that is used for edge detection. The edge, can be defined to lie anywhere along spline with a high gradient (Figure 3.3). To analyze this effect, the region along the spline with steep pixel intensity gradient was selected. The lower limit was obtained by averaging the pixel intensity for the darkest 4 pixels (Pixels 1-4 in Figure 3.3). This limit corresponds to the lowest illumination intensity where the drop can be located. A similar upper limt was set by the 4 brighest pixels (pixels 8-11 in Figure 3.3). However, from Figure 3.3, it is seen that there exists 5 pixels (7-11) that have the intensity of 255 and hence the resulting average of the 4 pixels would also be 255. To eliminate the possibility of an error that could occur when this average intensity is 255, the maximum value upper limit is set at 253. The resulting difference in drop edge co-ordinates as well as the contact angle was found to be miniscule and hence this approximation is considered valid. For situations when the average of the 4 brightest pixels is different from 255, the obtained average is set as the upper limit. Three more equally spaced locations were selected in the region between the upper and lower limits. Figure 3.2 shows the drop edge that is obtained for each approximation. The drop edge obtained by each method would move deeper into the drop as the pixel intensity level is lowered in the algorithm. For this reason, edge obtained by the approximation corresponding to *Position 5* is not appropriate for accurate contact angle determination, but is considered in the analysis.

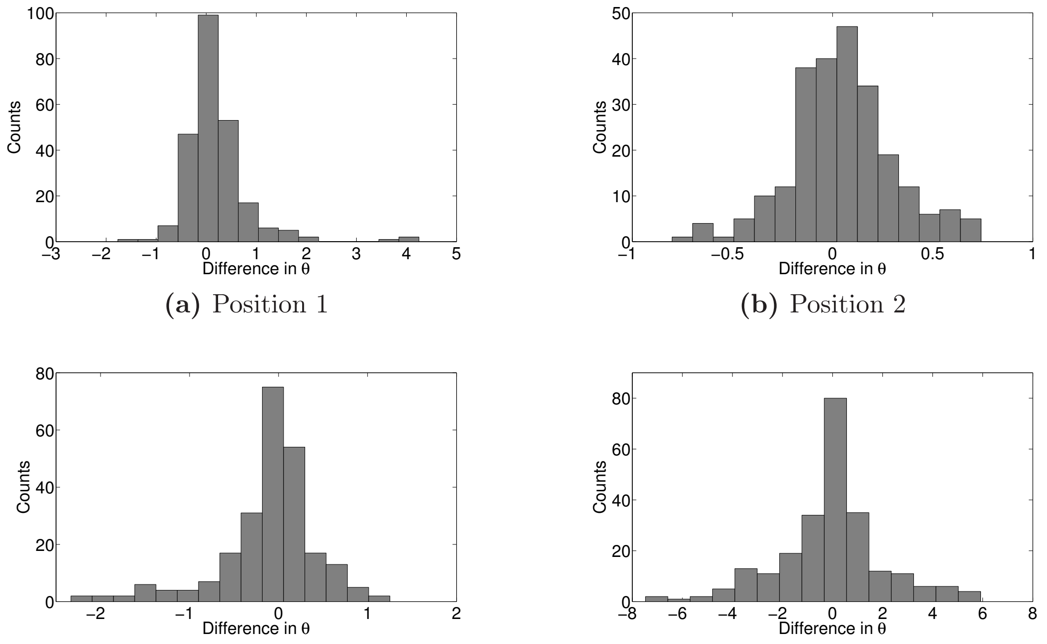

(a) Position 1 **(b)** Position 2

(c) Position 3 **(d)** Position 4

Figure 3.4. Distribution of $\Delta\theta$ between Position 3 and Positions 1, 2, 4 and 5 for samples in Table 3.1

Different sessile drop images with contact angle varying from 30° to 160° were selected and were processed with these approximations for edge detection and the corresponding contact angle for each method was obtained. Table 3.1 gives details of the samples used to obtain the images for this analysis. Figure 3.4 shows the distribution of error in contact angle that is obtained for positions *1, 2, 4 and 5* when compared with the contact angle obtained for *Position 3*. Table 3.2 summarizes the statistical parameters of the error in contact angle measurements. An explanation for this change in contact angle can be attributed to the change in the drop profile shape that occurs as different edge detection schemes are implemented. For the purpose of edge calculation, data points corresponding to *Position 3*, i.e. midway between the upper and lower limits, are selected following an analogy similar to Cheng et al. [1990].

Table 3.1. Samples used for pixel error estimation

Substrate	Fluid	Average obtained θ
Plexiglass	80% Tripropylene Glycol - 20% Water	38°±2
Plexiglass	40% Tripropylene Glycol - 60% Water	57.5°±1.8
Plexiglass	20% Tripropylene Glycol - 80% Water	67.5°±5.5
RainX	Water	100°±3
EGC1720	Water	109°±5
Toray	Water	158°±3

Table 3.2. Variation of Contact Angle with Edge Detection for samples in Table 3.1

	Mean Error	Standard Deviation	95% Region of Certainty	
			lower limit	Upper limit
Position 1	0.21	0.65	-0.86	1.28
Position 2	0.05	0.26	-0.38	0.48
Position 4	-0.11	0.55	-1.01	0.79
Position 5	-0.05	2.13	-3.33	3.45

3.3 Uncertainty in Exact Scale Calculation

The program `Scale` calculates the scale by analyzing the images of the stage micrometer. The program accounts for any vertical mis-alignments of the micrometer. However, pixelation of image creates an inherent error in scale calculation and the error is of the order ±1 pixel. To test the effect of this error on contact angle measurements, drop images with different contact angles were analysed by inducing error in the obtained scale. Error of ±1, ±2 pixels per millimeter was induced in the scale calculation and the results were compared with actual calculated scale.

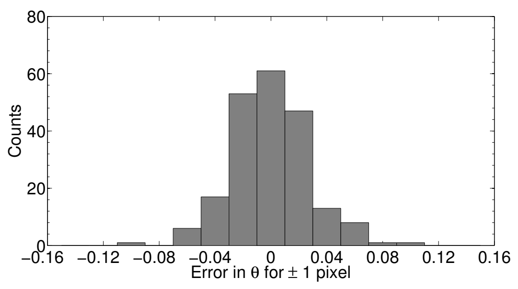

(a) ±1 Pixel

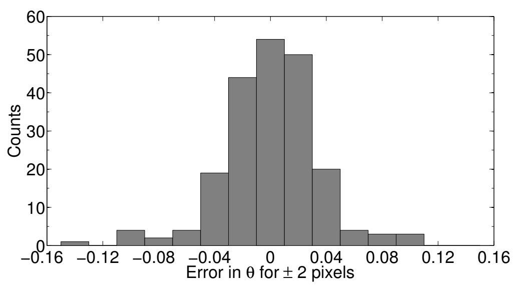

(b) ±2 Pixel

Figure 3.5. Error in Contact Angle Measurements with Error in Scale Calculation

Table 3.3. Variation of Contact Angle with Edge Detection

	Mean Error	Standard Deviation	95% Region of Certainty	
			Lower limit	Upper limit
±1 Pixel	3.2e-4	0.03	-0.05	0.05
±2 Pixels	5.5e-5	0.03	-0.06	0.06

Figure 3.5 shows the distribution of error of ±1 and ±2 pixels per millimeter, calculated against the contact angles obtained with no error in scale. Table 3.3 shows the statistical data for the same test. From the results it is evident that errors in the estimation of the scale for the drop images have no effect on contact angle measurements. This is because the the drops are non-dimensionalized using the capillary constant and it accommodates errors in absolute scale calculation. However, with an incorrect scale physical drop properties cannot be calculated accurately.

3.4 Illumination Control

Apart from estimation required to select the cutoff point for edge detection discussed in Section 3.2, the brightness of the source of illumination affects the obtained profile and hence the contact angle measured by ADSA. If the source is too bright, it causes the drop edge to move inside the drop when compared to the image with ideal brightness. To minimize this effect, an image of a needle of known outer diameter is taken and its diameter is measured. The gain of the camera is changed until the calculated diameter of the needle from the images compare to the actual diameter of the needle.

3.5 Solid-Liquid Interface Detection

The accuracy with which the solid-liquid interface, i.e. the surface of the substrate is detected plays a very important part in determining an accurate contact angle. After the fit between the Laplacian curve and the drop profile is made, the co-ordinates of the substrate's surface are used to cut-off the Laplacian curve and at this point the angle is calculated. For smooth surfaces, reflection from the surface aids in better detection of the solid-liquid interface (Figure 3.6a). The rough and porous surface of GDL makes it difficult to detect the interface (Figure 3.6b). In addtion, very high contact angles found on GDLs further hampers the ability to detect the exact interface and unless it becomes almost impossible to detect the interface within an accuracy of ±1 pixel.

An attempt has been made to test the effect of error in solid-liquid interface detection in contact angle measurement. For this purpose, theoretical drop profiles

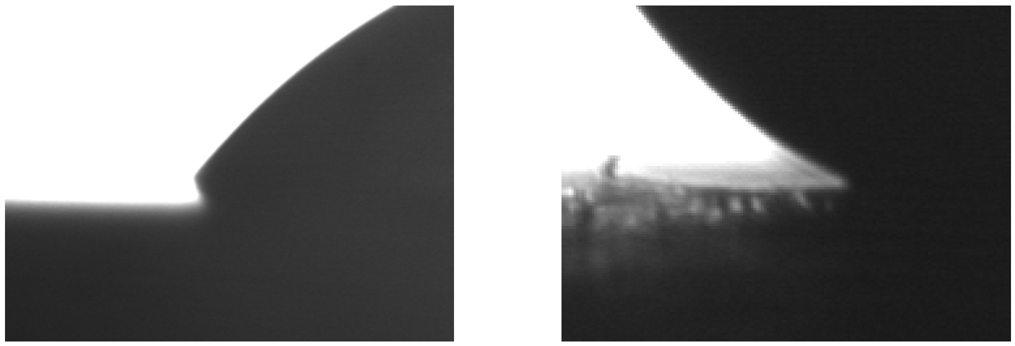

(a) Sessile Drop on Smooth Surface **(b)** Sessile Drop on GDL

Figure 3.6. Error in Contact Angle Measurements with Error Solid-Liquid Interface Detection. Scale = 2μm/pixel

were generated using different values of b. Error of ± 0.5 and ± 1 pixels was induced.. Error of -1 pixel indicate the location of interface was detected above the original location by 1 pixel. Simply, it means the drop height reduced by 1 pixel. Similarly, error of +1 pixel indicates an increase of 1 pixel in drop height.

Before the comparison is made, it is important to note that different magnifications used for capturing the drop images alter the dimensions of pixels in the image. Thus different drops will have a different resultant error even if they have a same magnitude of pixel error. The effect of inaccuracies in solid-liquid interface determination was calculated by generating drops of different sizes by varying b from 0.1 to 1 cm. Figures 3.7 and 3.8 show the error in contact angle calculation when the error in interface detection was varied from -1 pixel to +1 pixel. Figure 3.7 shows the error when the magnification is 2μm/pixel while Figure 3.8 corresponds to a magnification 5μm/pixel. These values of magnification were selected as they approximately represented the maximum and minimum magnification that could be obtained in the experiemental apparatus. A discrepency is seen in Figure 3.8d for $\theta = 170°$. This is because at $\theta = 170°$, an error of +1 pixel causes the resulting contact angle to exceed 180°. As 180° is the maximum contact angle that can exist, error is restricted to 10°. Following points can be asserted from these figures:

- For constant magnification and solid-liquid pair and the same error in interface estimation
  - Smaller drops result in a larger error as compared to bigger drops at constant contact angle.

  - Contact angle regimes of $\theta < 30^\circ$ and $\theta > 140^\circ$ are largely dependent on the accuracy of interface detection
  - Beyond θ=50° the calculated contact angle becomes highly sensitive to the calculated interface. In this regime, accurate calculation of the solid-liquid interface is of utmost importance.

- Higher magnifications, i.e., more pixels per mm yield a smaller error than lower magnifications

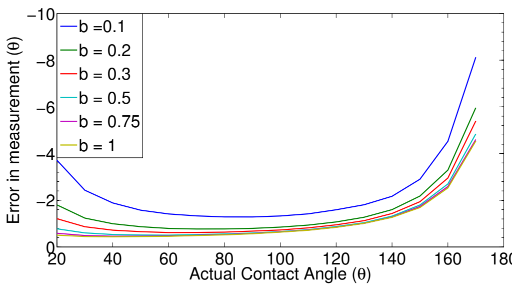

(a) -1 Pixel

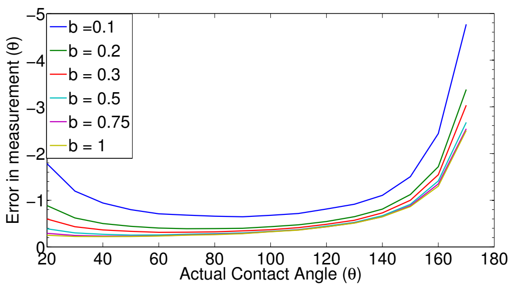

(b) -0.5 Pixel

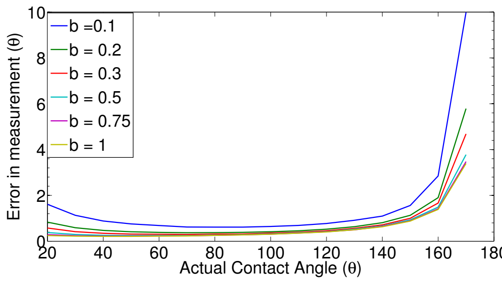

(c) +0.5 Pixel

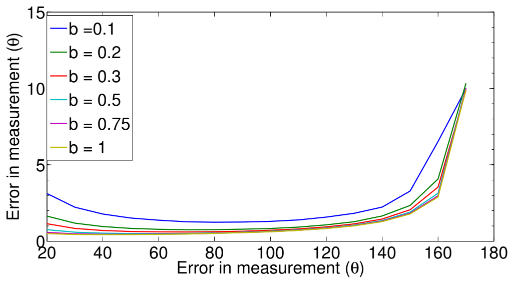

(d) +1 Pixel

Figure 3.7. Error in Contact Angle Measurements with Error Solid-Liquid Interface Detection. Scale = 2μm/pixel

In the program, the soild-liquid interface surface is calculated by finding the intensities of pixels normal to the surface. The pixel with maximum intensity gradient is then found along this normal. This procedure is repeated over the entire visible surface of the substrate (part of the substrate without the drop). A straight line is fitted to these points of maximum intensity gradients by the method of least squares. This line is approximated at the surface of the solid and the location where the drop profile intersects this line is the calculated solid-liquid interface. If the automated procedure fails to locate the solid-liquid interface, the program `images_reader` is run which allows the user to reposition the interface.

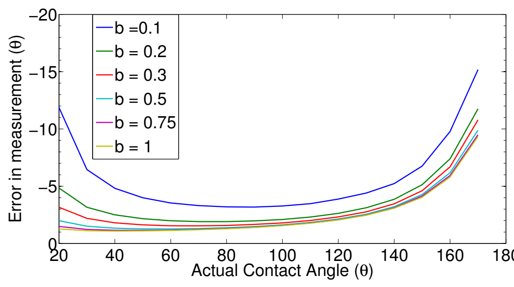

(a) -1 Pixel

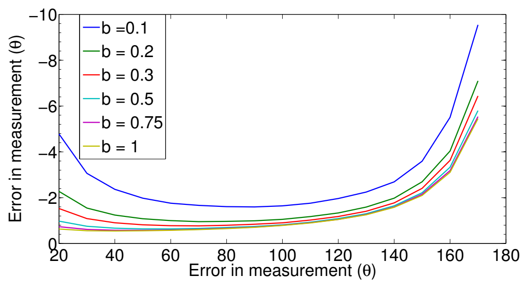

(b) -0.5 Pixel

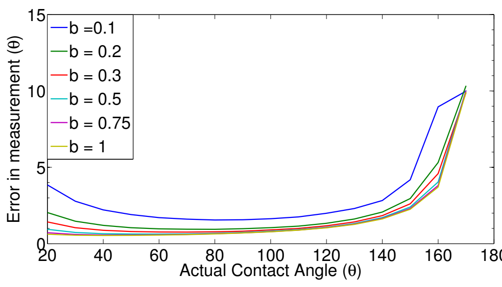

(c) +0.5 Pixel

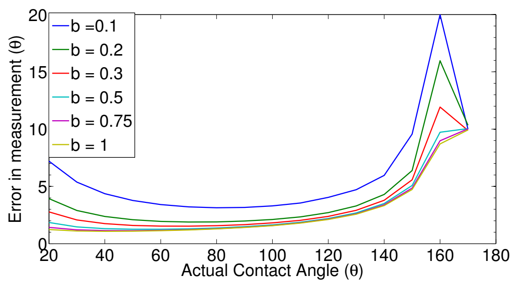

(d) +1 Pixel

Figure 3.8. Error in Contact Angle Measurements with Error Solid-Liquid Interface Detection. Scale = 5μm/pixel

Chapter 4. Experimental Procedure

4.1 Experimental Setup

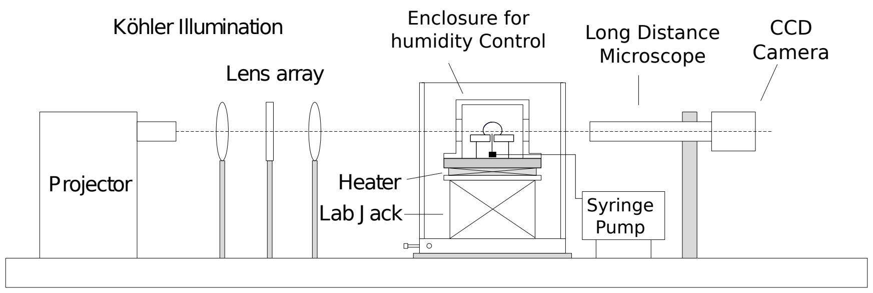

Figure 4.1. Schematic Diagram of experimental setup for ADSA

The contact angle measurement apparatus, shown in Figure 4.1, consists of a source of illumination, the stage to place the drops and a microscope coupled to CCD camera. Köhler illumination is used as it provides a beam of light of equal intensity. This helps in producing drop images with a good contrast between the drop and the background. The stage consists of an X-Y translation stage (Velmex AXY2509W1) on which a labjack (Thorlabs L200) is mounted which enables X-Y-Z movement. A long distance microscope (Infinity K2/S) is coupled to a CCD camera (PULNIX TM-1325CL). The camera is connected to framegrabber (EPIX EL1DB) and the images are captured using EPIX XCAP, a software that controls the camera on IBM Intellistation Z Pro (6223-7BU) workstation.

Figure 4.2 shows the stage of the experimental apparatus with the heat enclosure installed. The top of the stage consists of a copper block which is heated by four thermo-electric heaters (Marlow Industries DT12-6-01L). The temperature is controlled by varying the voltage across the heaters. The heat enclosure consists of two glass windows through which drop images are taken. The glass is coated with Indium-Tin Oxide which is heated by passing current through it. Heating of the glass prevents condensation of water vapor at higher temperatures on the glass when the enclosure is humidified.

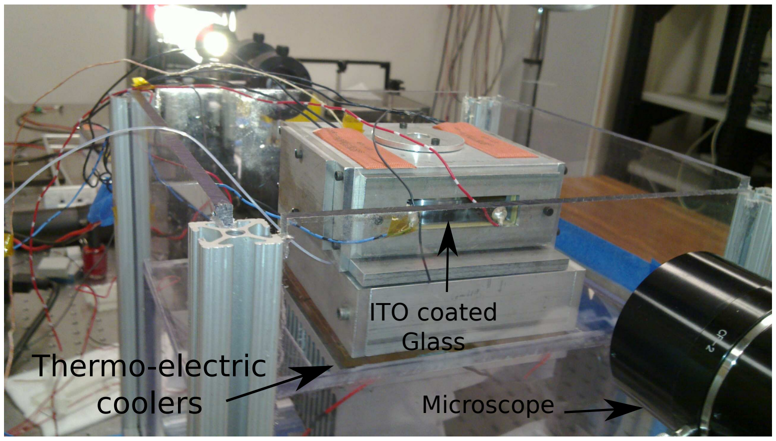

Figure 4.2. Image of the stage with enclosure

Figure 4.3 shows the setup that is used for the formation of advancing and receding drops on the GDL. This unit is placed inside the heat enclosure during dynamic contact angle measurements. Figure 4.3a shows the disassembled unit whereas Figure 4.3b shows the assembled unit with a GDL attached to the unit. The hypodermic needle is connected to a PTFE coated tubing. The other end of the tubing is coupled to the syringe pump.

Before the drop images are taken, a scale factor is needed to identify the dimension of the drop. For this purpose, after the magnification and the focus of the microscope is set, an optical micrometer (Larman Rulings KR 812) is placed on the stage at the focal point of the microscope and an image of the micrometer is captured. This image is used to calculate the scale factor and hence determine the dimensions of the drop.

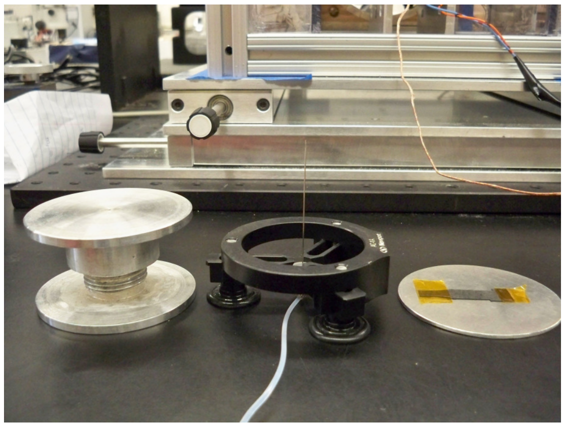

(a) Liquid Injection Setup (Disassembled)

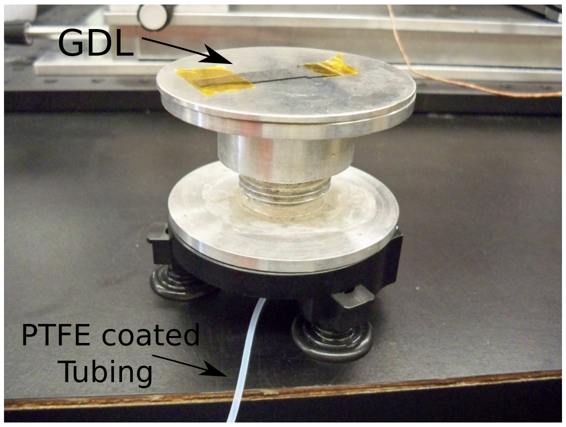

(b) Liquid Injection Setup (Assembled)

Figure 4.3. Setup for liquid infusion and withdrawl

4.2 Static Measurement

To measure the static contact angle, a drop of liquid is formed on the tip of the hypodermic needle attached to a screw syringe. The syringe is fastened to a stand which reduces any irregularities that are produced by manual drop deposition. The substrate is then raised till it touches the drop using the Y control of the stage. The drop is the then brought into the field of view and onto the focal point of the microscope by x-y translation of the stage and image is captured.

4.3 Dynamic Contact Angle Measurement

For measurement of advancing contact angle, syringe pump is used to inject fluid continuously at a constant rate. The GDL substrate is attached to the top of aluminum plate using Kapton tape. A small hole is punched on the GDL. The size of the piercing is kept close to the diameter of the needle used for injecting the liquid. This is done as safety precaution to prevent the fluid from seeping through the hole and beneath the GDL. A series of images is captured at constant time rate from which advancing contact angles are obtained. At the end of the sequence, the syringe pump is reversed and water is withdrawn from the drop.

4.4 Humidity Control

As the temperature increases the amount of water vapor in the air needed for saturation increases. If the air is not humidified, the water drops formed for measurements will evaporate and hence the obtained contact angle will deviate from the actual one. Humidity is increased by placing water filled containers in the heat enclosure. To check and the rate of evaporation, a very small droplet of water (approximately 2-3μl) is injected in the chamber at set temperature and the time required for the drop to evaporate is measured. Evaporation rate of less than 0.5μl/min, was considered satisfactory for the experiment to be carried on.

Sessile drops are formed by injecting water through a small hole in the GDL substrate by a hypodermic needle. Teflon tubing is used to pass water from the syringe to the needle. The temperature of the enclosure is increased by increasing the voltage across the thermo-electric heaters. Once the plate, on which the GDL substrate is kept, reaches the desired temperature, the voltage is kept constant and the enclosure is kept in the same state for a period of 20-30 min. This allows the entire chamber to attain an equilibrium temperature. Around 5-6 inches of the tube is present in the heat chamber and is in contact with the heated copper plate allowing the water to attain the equilibrium temperature. This ensures the temperature of water is same as that of experimental temperature.

Chapter 5. Results

With aim to understand the wetting characteristics of fuel cells, different GDL samples were tested under static and dynamic conditions and also at different temperatures. The GDL samples with composition are shown in Table 5.1. SEM images of the tested samples in shown in Figure 5.1. PTFE coating in the samples is seen as the webbing in between the fibers. Apart from Freudenberg which has intertwined structure, all other samples consists of carbon fibers. Pore size distribution for three samples is shown in Table 5.2.

Table 5.1. GDL samples tested

Baseline	Mitsubishi MRC 105 9% PTFE (weight) with MPL
SGL	SGL 25 BC
Freudenberg	Freudenberg H2315 with MPL
Toray	Toray TFP-H-060 7% PTFE

Table 5.2. Pore size distribution of the tested GDL samples (Nishith Parikh, MTU, unpublished data)

	SGL	Freudenberg	Toray
Average Pore Radius (μm)	8.25	15.92	13.2
Standard Deviation	8	19.5	9.75

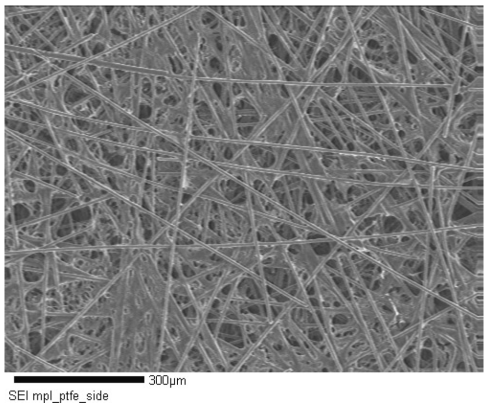

(a) Mitsubishi

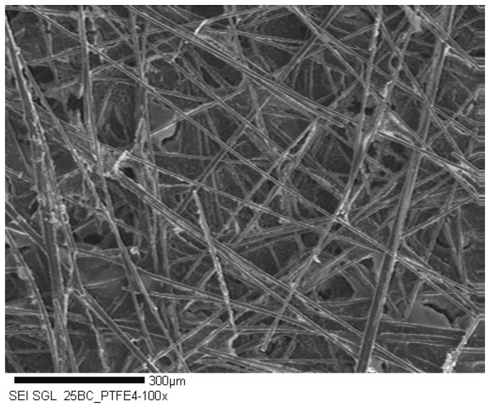

(b) SGL

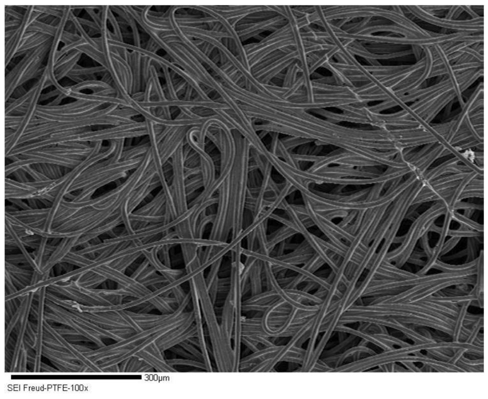

(c) Freudenberg

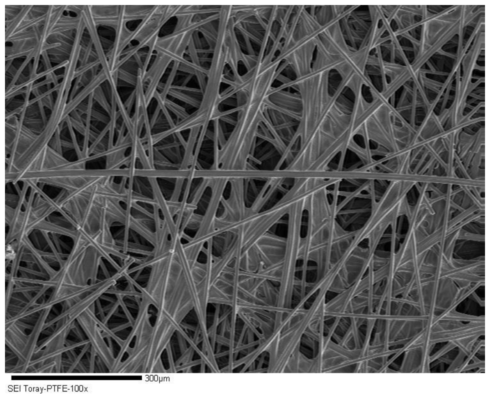

(d) Toray

Figure 5.1. SEM images of GDL samples tested for contact angle measurement

5.1 Asymmetry in Drop Profile

The surface of a GDL is highly rough and porous. The contact angle obtained on such a surface becomes dependent on the profile of the surface where the drop is deposited. This results in different contact angles on the left and right side of the drop. Figure 5.2 shows the image of a water drop on Toray obtained during advancing contact angle measurements. From the figure, it is seen that the contact angle at the left side of the drop is lower than the angle on the right side of the drop. During dynamic contact angle measurements, in many runs, pinning of the drop on one side occured while the movement of the contact line would take place on the other side. For such cases, only the data on the side with contact line movement is considered.

Table 5.3. Difference in Contact Angle for Left and Right Side of Drop. Fluid: Water, Substrate: Toray

Temperature (˚C)	Equatorial Radius (cm)	θ Left	θ Right	Difference in θ
25	0.109	153.8	152.7	1.1
	0.088	153.7	151.9	1.8
	0.11	156.2	153.1	3.1
	0.100	154.0	155.8	1.8
	0.124	151.8	154.0	3.2
55	0.080	153.9	152.5	1.6
	0.127	158.0	153.5	4.5
	0.089	152.1	151.7	0.4
	0.088	154.5	153.9	0.6
	0.923	154.8	155.5	0.7
85	0.086	154.2	152.8	1.1
	0.103	153.7	156.4	0.7
	0.093	154.6	155.8	1.2
	0.096	153.1	153.7	0.6
	0.089	153.3	151.7	1.6

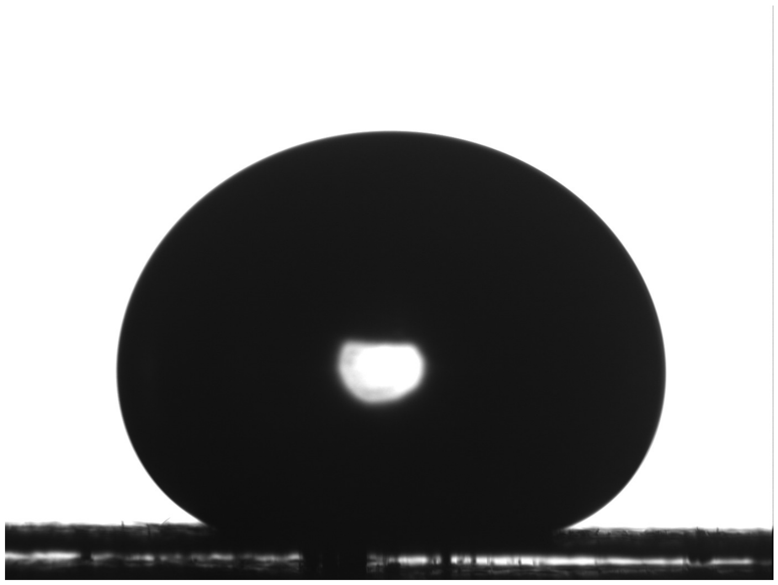

Figure 5.2. Difference in θ between left and right side of drop

5.2 Static Contact Angle Data

The static contact angle was measured on GDLs using the technique explained in 4.2. Figure 5.3 shows the observed variation in contact angle with respect to the equatorial radius at different temperatures. The mean contact angle obtained for the four GDL samples at different temperatures is shown in Table 5.4. Extremely rough and porous surface of the GDLs results in large hysteresis. Depending upon the placement of the drop, the contact area as well as the contact line develop different configurations and causes this hysteresis. Also some of the fibers protruding from the surface create additional contact zones over the drop surface altering the drop into an asymmetric drop. In such asymmetric drops, the obtained contact angle is then dependent on the cross-section plane of which the image was taken, as along different cross-sections different profiles would be obtained. Miller et al. [1996] and Veeramasuneni et al. [1997] observed an increase in both advancing and receding contact angles for thin film PTFE coatings with increasing roughness in nanoscale regime. However, the only data that is availble pertaining to the structure of GDLs is the pore size distribution and from the results, concrete conclusion cannot be drawn regarding the drop size or temperature dependence of contact angle on GDL.

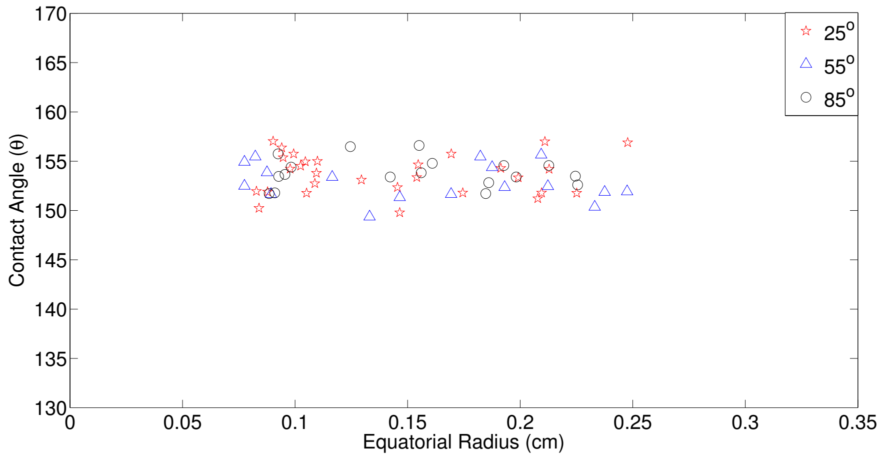

Figure 5.3. Static Contact Angle on Baseline vs temperature

Table 5.4. Mean static contact angle on GDLs at different temperatures

GDL	25° C	55° C	85° C
Mitsubishi	154.2 ±3	154.8 ±3.5	154.3 ±3.5
SGL 25BC	151.7 ±4	149.1 ±4.5	150.5 ±3
Freudenberg	148.2 ±4.5	147.5 ±5	145.8 ±4.5
Toray T060	154.7 ±3	153.6 ±2.5	154.3 ±2

5.3 Dynamic Contact Angle on GDL

Advancing and receding contact angles were measured on the samples and the results are plotted in Figure 5.5 through 5.12. Figure 5.4 shows the variation in contact angle that was observed when multiple runs were carried out on the same sample. Different runs result in a wide range of advancing contact angles for the same sample, the cause of which can be attributed to reasons explained previously in Section 5.2. On Baseline, Freudenberg and Toray, lower advancing contact angles were obtained at higher temperatures. On SGL, a similar behavior is observed for smaller drops. However at larger drop size, this change became negligible. Low contact angles observed on Baseline and Toray for small drop sizes is observed because of the contact line being pinned and the drops size being increased.

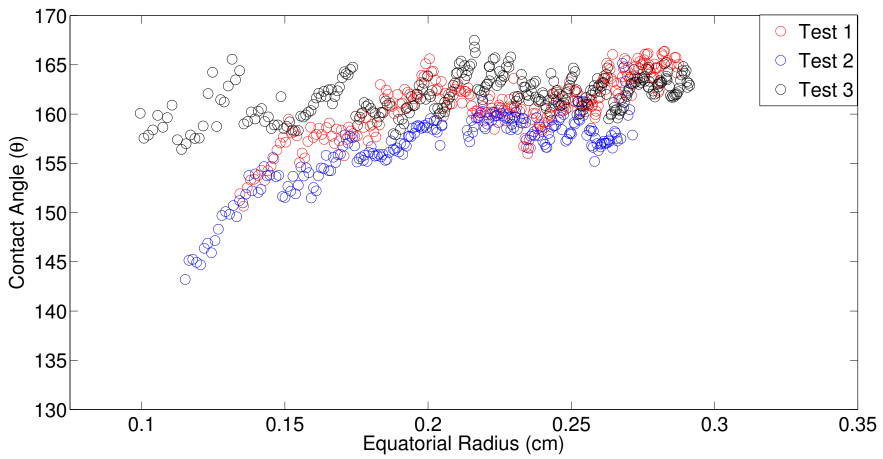

Figure 5.4. Advancing Contact Angle on Toray obtained for 3 test runs at 25° C

The receding contact angles however show a definite reduction in contact angle as the temperature is increased. As the drop volume is reduced, the contact line would move towards the needle. But beyond a certain point, it would be pinned

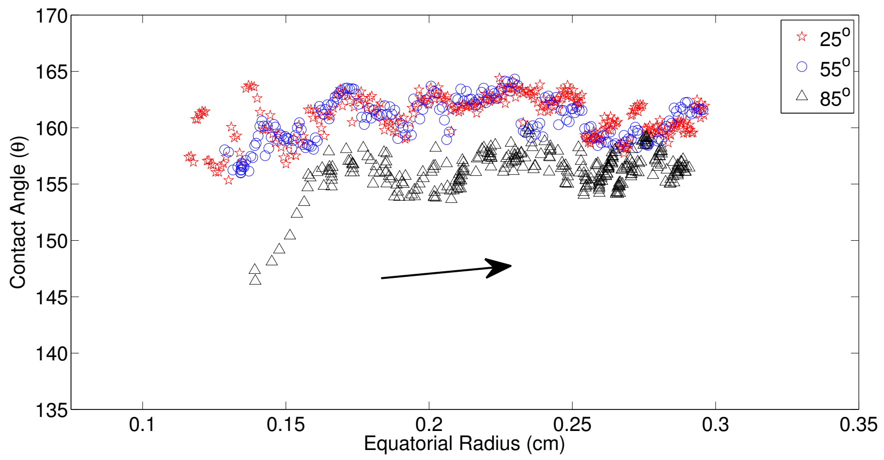

Figure 5.5. Advancing Contact Angle on Mitsubishi vs temperature

and the angle would keep reducing. This phenomenon was more evident at higher temperature.

For a Cassie drop with air trapped in the pores, the hysteresis is much less as compared to a Wenzel drop (He et al. [2004] and Marmur [2004]) as the drops rests on the peaks of rough surfaces, whereas in Wenzel wetting, the drops are heavily pinned. From the results, a large difference between the advancing and receding

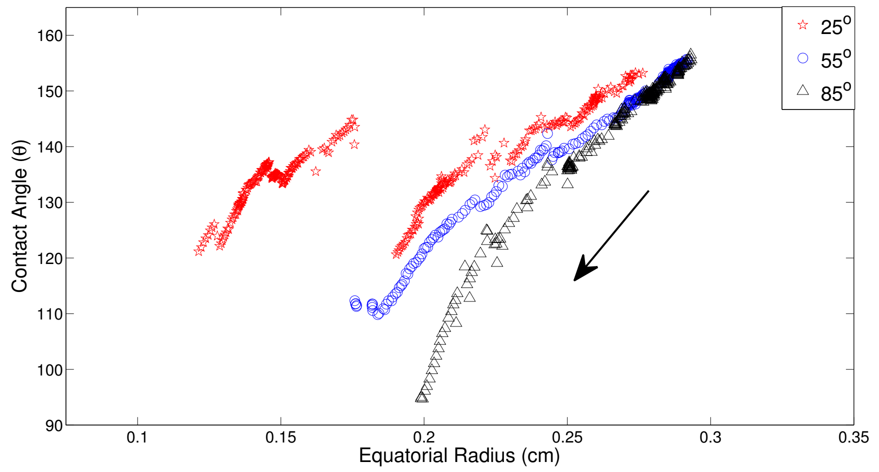

Figure 5.6. Receding Contact Angle on Mitsubishi vs temperature

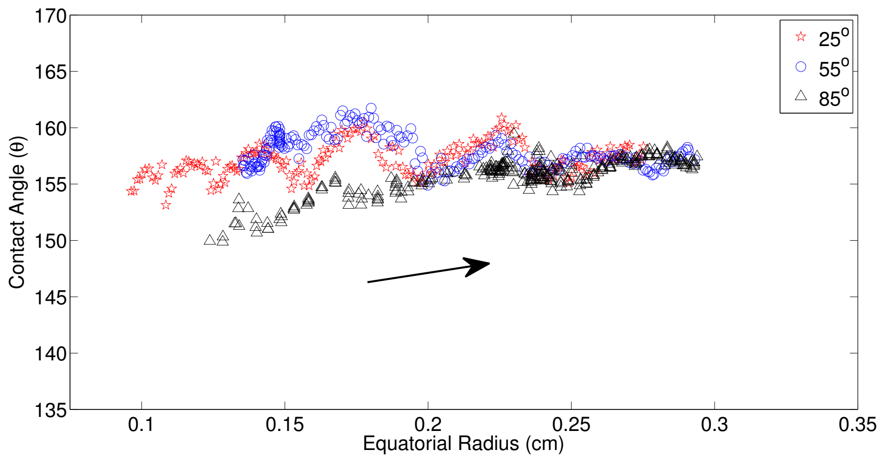

Figure 5.7. Advancing Contact Angle on SGL vs temperature

contact angles is observed and hence Wenzel wetting occurs on GDLs. This type of wetting is also expected during the operation of fuel cell as water droplets are formed in the pores and on the GDL.

Another observation that was made during experiments was the vibration of sessile drops on hydrophobic GDLs at larger drop volumes. For a sessile drop with high contact angle, a large volume of the drop is supported on a small contact area. At

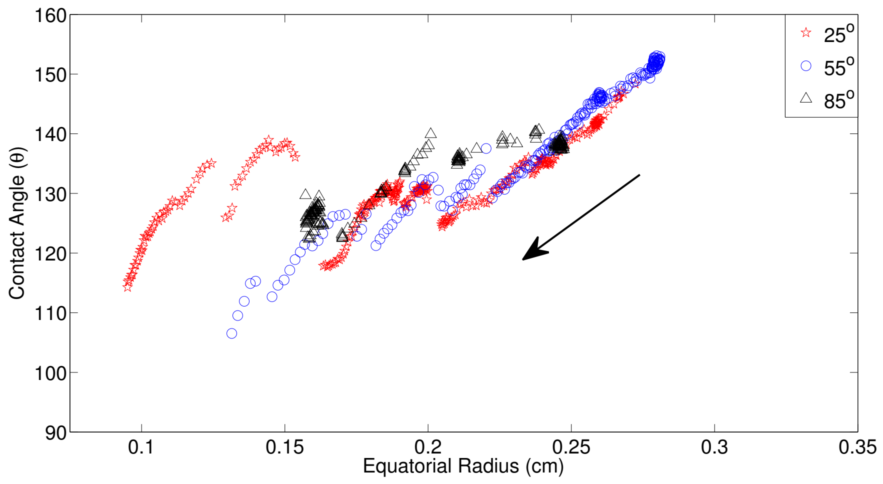

Figure 5.8. Receding Contact Angle on SGL vs temperature

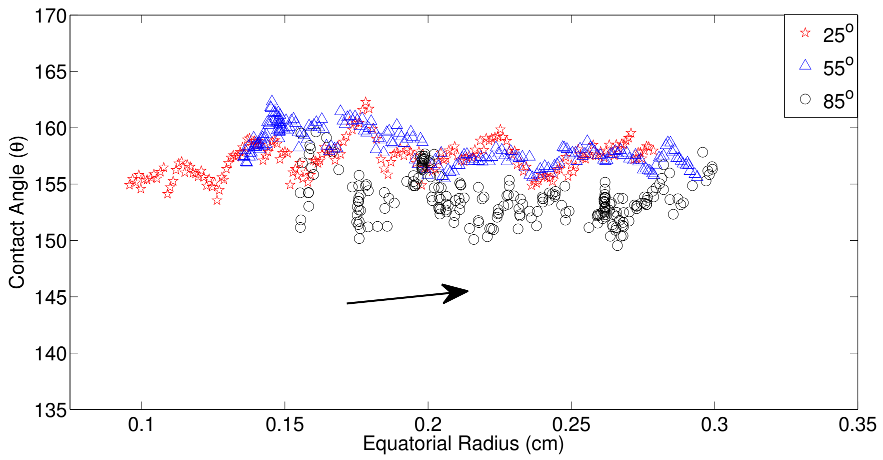

Figure 5.9. Advancing Contact Angle on Freudenberg vs temperature

high drop volumes, typically 50-60 μl and above, the drop starts to vibrate because of the small vibrations that exists in the stage. This produces a large variation in the measured contact angle at high drop volumes.

Receding contact angle at 25 °C on Mitsubishi GDL in Figure 5.6 is replotted in Figure 5.13c. A large discontinuity in contact angle is visible between the data points at A (Figure 5.13a) and B (Figure 5.13b). Smaller discontinuities are also visible

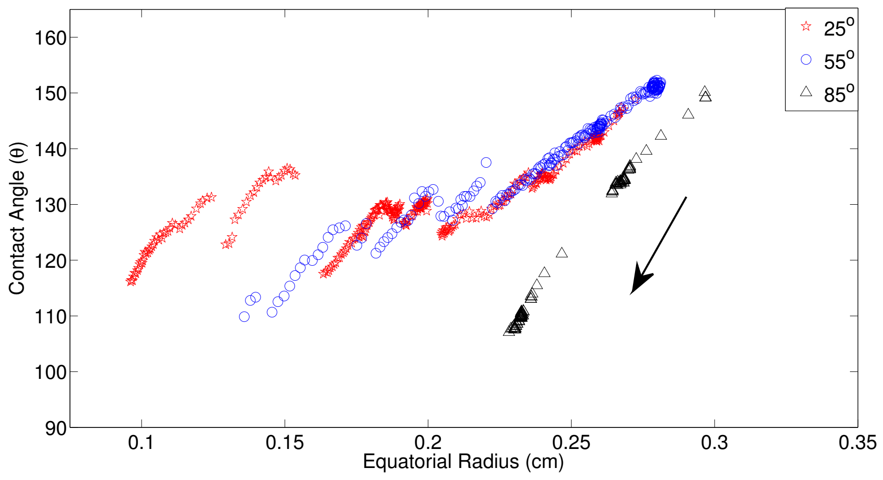

Figure 5.10. Receding Contact Angle on Freudenberg vs temperature

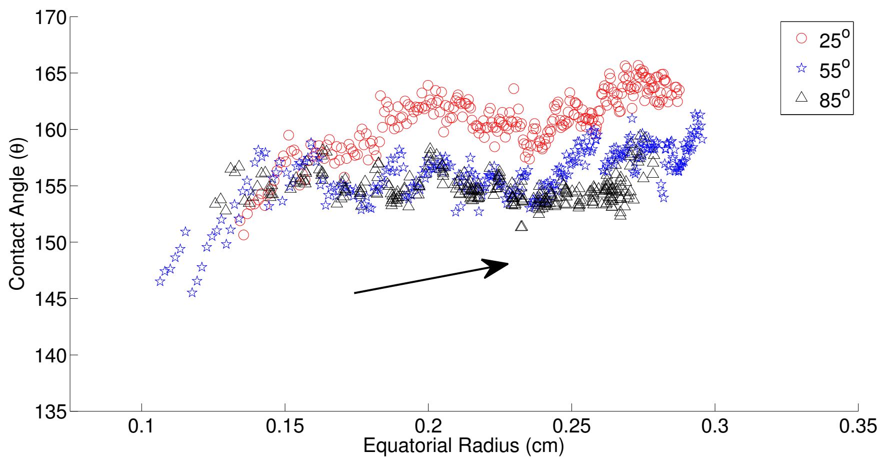

Figure 5.11. Advancing Contact Angle on Toray vs temperature

at points *C*, *D* and *E*. These jumps in contact angles occur when the contact line moves rapidly from one position to another as the drop volume is reduced. Such a variation in contact angle due to rapid contact line motion is seen on other GDLs as well. Movement of the contact line also affect the advancing contact angle and it manifests as the wavy or oscillatory trend in advancing contact angles. If the contact line is pinned or moves slowly, increase in the drop volume results in an increase in

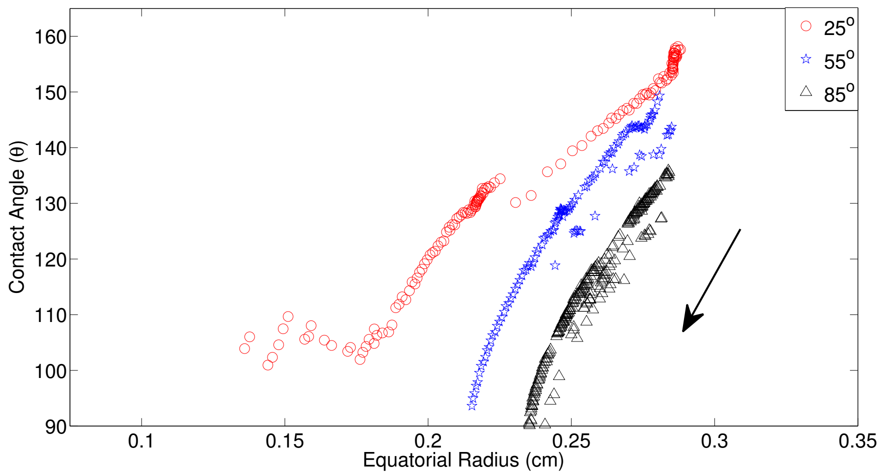

Figure 5.12. Receding Contact Angle on Toray vs temperature

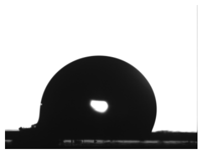
(a) A

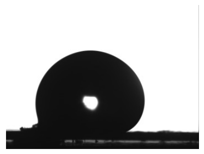
(b) B

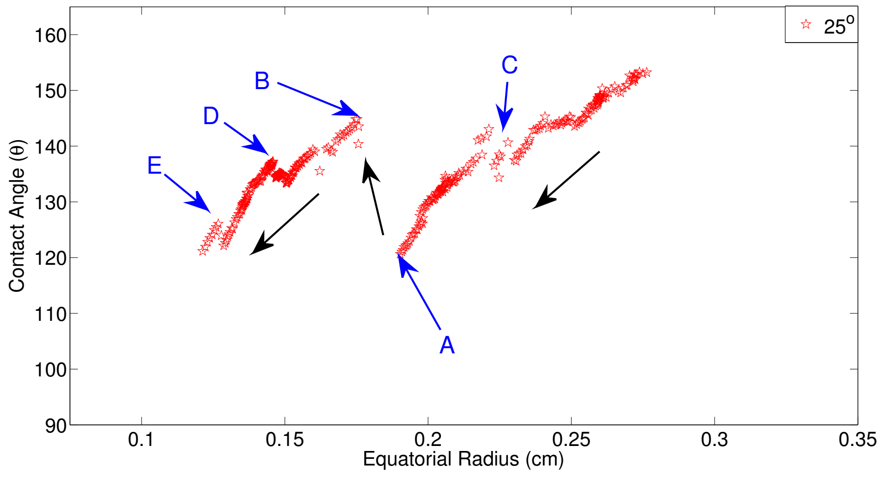

(c) Receding Contact Angle on Mitsubishi

Figure 5.13. Receding Contact Angle on Mitsubishi

the contact angle. Beyond a certain value, represented by the ‘peaks’, the contact line moves rapidly which causes the contact angle to reduce. This phenomenon repeats resulting in the oscillatory nature of the advancing contact angles.

Chapter 6. Conclusion

6.1 Summary

A program to determine the contact angle has been developed in MATLAB®. The program is automated to analyze multiple images which enables the calculation of advancing and receding contact angles. The contact angles are determined by fitting an ideal sessile drop profile curve obtained from the Laplace-Young equation with the drop edge profile obtained from the drop images. The existing setup for the measurement of contact angles was modified to incorporate a heat enclosure to maintain the humidity at higher temperatures, which is necessary to prevent droplet evaporation. The new setup allows for injection and removal of water on the surface of GDL from which advancing and receding contact angles are obtained. Also, these measurements were performed at different temperatures.

Accuracy in contact measurement is dependent on the drop deposition method, drop profile acquisition method and the accuracy in determining the solid-liquid interface. For drops with contact angles less than 90°on a smooth surface, solid-liquid interface in determined with high accuracy making the results more accurate. For GDLs, the high contact angles coupled with porous and rough fibrous surface restricts the accuracy in determining the contact angles.

Pixelation of drop images induces uncertainty in the contact angle measurement. As the drop edge obtained from image processing deviates more from the actual drop profile, the uncertainty increases. Incorrect scale calculations produce no effect on the contact angle obtained from images. At high contact angles, the inability in exact solid-liquid interface detection further increases the error.

Advancing and receding and contact angles were collected for four GDL samples at three different temperatures. Contact angle hysteresis that exists on GDL samples hinders any concrete conclusion to be drawn from the experimental results for advancing measurements. Advancing Contact angles obtained from multiple runs on GDLs result in a wide range of values which are comparable to that obtained at other temperatures. A decrease in receding contact angle is observed as the temperature is increased in all samples except SGL. Static contact angles obtained on GDL are dependent on the drop deposition technique.

6.2 Recommendations

Experiments to measure contact angles on GDLs should be performed with care and precision as the hysteresis produces a large variation in results. For a better understanding of the wetting characteristics of the GDLs more experiments need to be performed. This will allow a better statistical analysis of wetting in GDLs. Also, the experiments were performed on new or unused samples. Similar experiments should be conducted on 'end-of-life' samples as it may be helpful in understanding the changes that take place in the wetting characteristics of GDLs during the life cycle.

APPENDICES

Appendix A. Abbreviations

θ	Contact angle
θ_a	Advancing contact angle
θ_r	Receding contact angle
θ_C	Cassie-Baxter's contact angle
θ_Y	Young's contact angle
θ_W	Wenzel's Contact Angle
ρ	Density
σ	Surface tension
σ_{LV}	Liquid-vapor interfacial tension
σ_{SL}	Solid-liquid interfacial tension
σ_{SV}	Solid-vapor interfacial tension
ADSA	Axisymmetric Drop Shape Analysis
b	Radius of curvature at apex
B	Non-dimensional radius of curvature at apex
Bo	Bond number
c	Capillary constant
f	Fractional Area
g	Gravitational constant
GDL	Gas Diffusion Layer
p	Perimeter
ΔP	Change in pressure
ΔP_g	Change in hydrostatic pressure
ΔP_σ	Change in pressure across curved interface
PEM	Proton Exchange Membrane
PTFE	Polytetrafluoroethylene
R_1	First principal radius of curvature
R_2	Second principal radius of curvature
r	Roughness factor
s	Arc Length of drop surface
S	Non-dimensional arc Length of drop surface

ΔW	Change in weight
x	Horizontal distance
X	Non-dimensional horizontal distance
z	Vertical distance
Z	Non-dimensional vertical distance

Appendix B. Contact Angle Measurement Programs

2.1 scale

```
% This function creates sc.mat which contains the scale factor for the
% drop images. Enter the number of scales taken and import them.

% First zoom the images and select a suitable point on the leftmost line
% which has uniformly varying pixel intensity. Then select the top or the
% bottom part of the same line used initially. Do the same for rightmost
% line. Enter the scale im mm for each image

%%

a = input('enter number of scales');  % Enter the number of scale images.
scale_img = zeros(1,a);
pix_ind_x = -7:1:7;                   % Pixels used for spline fit in x

nop = 30;
for j = 1:a

    pix_x = zeros(nop,length(pix_ind_x));
    pix_z = pix_x;

    % Opens filepath of previously opened folder
    oldpath=char(textread('filepath.dat','%s','whitespace',''));

    % Lets user select full filepath of image graphically
    [filename,filepath]=uigetfile([oldpath,'*.tif'],'open file:');
```

```
fid=fopen('filepath.dat','w');
fprintf(fid,'%s',filepath);
fclose(fid);

% Saves image to 'scale_fig' from specific filepath as selected
   above
scale_fig = imread([filepath,filename]);

figure, imshow(scale_fig, [])

x_top = zeros(1,2);                 % x coordinate of top/bottom
z_top = zeros(1,2);                 % z coordinate of top/bottom

for k = 1:2
    figure, imshow(scale_fig, [])
    pause(7);
    if k == 1
        [xl, zl]=ginput(1);               % Select scale points
    else
        [xr, zr]=ginput(1);               % Select scale points
    end
    pause(5)
    [x_top(k) z_top(k)] = ginput(1);     % Select top point for
       tilt
end

x_l(1:nop) = (xl-(nop/2)+1):1:(xl+nop/2);
z_l(1:nop) = zl;
x_r(1:nop) = (xr-(nop/2)+1):1:(xr+nop/2);
z_r(1:nop) = zr;

pixel_index_l = zeros(nop,length(pix_ind_x));  % Pixel intensity
   saved here
pixel_index_r = zeros(nop,length(pix_ind_x));  % Pixel intensity
   saved here

for k = 1:nop
    pix_x_l(k,1:length(pix_ind_x)) = round(x_l(k)) + pix_ind_x;
    pix_z_l(k,1:length(pix_ind_x)) = round(z_l(k));

    for m = 1:(length(pix_ind_x))
        pixel_index_l(k,m) = double(scale_fig(pix_z_l(k,m),
           pix_x_l(k,m)));
    end
end

for k = 1:nop
    pix_x_r(k,1:length(pix_ind_x)) = round(x_r(k)) + pix_ind_x;
    pix_z_r(k,1:length(pix_ind_x)) = round(z_r(k));
```

```

        for m = 1:(length(pix_ind_x))
            pixel_index_r(k,m) = double(scale_fig(pix_z_r(k,m),
               pix_x_r(k,m)));
        end
    end

    tilt = atand((z_top(2)-z_top(1))/(x_top(2)-x_top(1)));
    multiplier = (z_top(2)-z_top(1))/cosd(tilt)-(z_top(2)-z_top(1));

    n_pts = length(pix_ind_x);
    x_opt_l = zeros(1,nop);
    x_opt_r = zeros(1,nop);

    % Fits a spline curve and finds location of minimum pixel
       intensity
    for k = 1:nop
        base_pts_x = linspace(pix_x_l(k,1),pix_x_l(k,end),(n_pts*100)
           +1);
        spline_fit_x = spline(pix_x_l(k,:),pixel_index_l(k,:),
           base_pts_x);
        x_opt_l(k) = base_pts_x(find((spline_fit_x) == min(
           spline_fit_x),1,'first'));
    end

    for k = 1:nop
        base_pts_x = linspace(pix_x_r(k,1),pix_x_r(k,end),(n_pts*100)
           +1);
        spline_fit_x = spline(pix_x_r(k,:),pixel_index_r(k,:),
           base_pts_x);
        x_opt_r(k) = base_pts_x(find((spline_fit_x) == min(
           spline_fit_x),1,'first'));
    end

    for k = 1:nop
    pixels(k) = x_opt_r(k)-x_opt_l(k);
    end
        mm     = input('Enter size of scale in mm: ');
    cm     = mm/10;

    scale_all = zeros(nop,1);

    for k = 1:nop
    scale_all(k)=(abs(pixels(k)/cm))+((abs(z_top(2)-z_top(1)))/(abs(
       x_l(k)-x_r(k))))*multiplier;
    end
    scale_img(1,j) = mean(scale_all);
end
```

```
save sc.mat scale_img;
% eof
```

2.2 needle_Scale

```
clc
clear
close all
no_p = 41;                %Max permitted value 100
k = 1;

filepath =  'C:\ABCD\ABCD\';   % Enter filepath
filename = ('needle.tif');     % Enter filename

needle_img_uint  = imread([filepath,filename]);

needle_img = double(needle_img_uint);
figure, imshow(needle_img, [])

pause(5)
[x, z]=ginput(4);

%% For left side
Z_l = (round(z(1)):1:round(z(2)));
Z_r = (round(z(3)):1:round(z(4)));

X_l = round((x(1)+x(2))/2);
X_r = round((x(3)+x(4))/2);

for j = 1:length(Z_l)

    pixel_ind = X_l+ ((-no_p):1:(no_p));

    for k = 1:(no_p*2+1)
    pixel_data(k) = needle_img(Z_l(j),pixel_ind(k));
    end

    ind = find(pixel_data ≤ 80,1,'first');

    mean_top = mean(pixel_data(1:ind));

    mean_bot = mean(pixel_data((ind+1):end));

    avg_int  = (mean_top+mean_bot)/2;

    base_pts = linspace(pixel_ind(1),pixel_ind(end),(no_p*200));
    spline_fit = spline(pixel_ind,pixel_data,base_pts);

    diff_int = abs(avg_int - spline_fit);
    x_l(j) = base_pts(find(min(diff_int)==diff_int));

    k = k+1;
end

%% For right side

for j = 1:length(Z_r)

    pixel_ind = X_r+ ((-no_p):1:(no_p));

    for k = 1:(no_p*2+1)
    pixel_data(k) = needle_img(Z_r(j),pixel_ind(k));
    end


    ind = find(pixel_data ≤ 80,1,'first');

    mean_top = mean(pixel_data(1:ind));

    mean_bot = mean(pixel_data((ind+1):end));

    avg_int  = (mean_top+mean_bot)/2;

    base_pts = linspace(pixel_ind(1),pixel_ind(end),(no_p*200));
    spline_fit = spline(pixel_ind,pixel_data,base_pts);

    diff_int = abs(avg_int - spline_fit);

    x_r(j) = base_pts(find(min(diff_int)==diff_int));

    k = k+1;
end

x_mean_l = mean(x_l);
x_mean_r = mean(x_r);

scale_pic = x_mean_r - x_mean_l;

load sc.mat

Diamater_needle = scale_pic/scale_img

% eof
```

2.3 Contact Angle Measurement Program

```
% Main program for contact angle measurement

clear
close
clc

%% Load scale
load sc.mat             % loads previously saved scale
S_span=(0:.0001:3.5);   % S_span is the step variable for ode45 solver

%% Analysis parameters
% These parameters affect the number of points and their location on
   drop profile where calculations are done

No_ind    = 21;       % No of points where fit is calculated;
No_pt_slp = 16;       % No of pts used for quadratic fit on each side
dif_slp   = 3;        % Difference in pixels for slope calcutation
cut_off   = 17;       % difference between the end pt on the drop and
   last pt where error is calculated

%% Load properties and images

total_imgs = input('Enter total number of images');  % Number of
   images
total_scl  = input('Enter total number of scales');  % Number of
   scales

expt_type = input('Entrer the type of experiment: 1—Static, 2—
   Advancing');  % Type of Experiment
prefix_img = input('Enter a prefix if it exists (Press Enter if
   nothing exist)');  % Prefix to image number
start_no_img = input('Enter Image Start Number');  % Number of 1st
   image
range_lim = input('Range of images: For 1—10 Enter 1 For 11—99 Enter
   2 For 101—999 Enter 3  '); % The Range of images
file_location = input('Enter Filepath (ex: C:\Folder\Folder\
   Image_Folder\) :','s')';   % Location of images
file_location = file_location';

d_side = input('Enter side for More accuracy: Left = 1, Right = 2,
   Both = 3 : ');  % The side where more accuracy is needed

A = struct('scale_i',{},'folder_i',{},'file_i',{},'x_data_all_i',{},'
   z_data_all_i',{},'x_l_i',{},'z_l_i',{},'x_r_i',{},'z_r_i',{},'
   apex_x_i',{},'apex_z_i',{},'xpl_i',{},'zpl_i',{},'xpr_i',{},'zpr_i
```

```
    ',{}); % Structure for variables

Data = zeros(total_imgs,13);          % Variable to store data
Err_data = zeros(total_imgs,72);      % Variable to store data


for i = 1:total_imgs
    [I,A(i).folder_i,A(i).file_i] = image_input(i,expt_type,
       prefix_img,start_no_img,range_lim,file_location);   % Images
       input here
    [BW,A(i).IC_i]                  = image_analysis(I);  % Image
       converted to Black and White
    [boundary]                      = edge_detector(BW);  % Boundary of
        drop
    [mean_l,mean_r,A(i).xpl_i,A(i).xpr_i,A(i).zpl_i,A(i).zpr_i ] =
       plane( A(i).IC_i,boundary ); % Detects the solid-liquid
       interface
    [A(i).x_data_all_i,A(i).z_data_all_i,A(i).x_l_i,A(i).z_l_i,A(i).
       x_r_i,A(i).z_r_i,A(i).apex_x_i,A(i).apex_z_i] = profile_split(
       boundary,mean_l,mean_r); % Data points obtained
    close all
    display(A(i).file_i);
    if total_scl > 1
        scl = input('Enter scale number');
        A(i).scale_i = scale_img(scl);
    else
        A(i).scale_i = scale_img(1,1);
    end
end

clear I_sobel I BW boundary

%% Main loop

for r = 1:total_imgs

    folder       = A(r).folder_i;
    file         = A(r).file_i;
    scale        = A(r).scale_i;
    IC           = A(r).IC_i;
    x_data_all   = A(r).x_data_all_i;
    z_data_all   = A(r).z_data_all_i;
    x_l          = A(r).x_l_i;
    z_l          = A(r).z_l_i;
    x_r          = A(r).x_r_i;
    z_r          = A(r).z_r_i;
    apex_x       = A(r).apex_x_i;
    apex_z       = A(r).apex_z_i;
    xpl_i        = A(r).xpl_i;
```

```
zpl_i         = A(r).zpl_i;
xpr_i         = A(r).xpr_i;
zpr_i         = A(r).zpr_i;


%%  Indices of the points for left profile

ind_l = floor(0:((length(x_l)−cut_off)/(No_ind−1)):(length(x_l)−
    cut_off));
ind_r = floor(0:((length(x_r)−cut_off)/(No_ind−1)):(length(x_r)−
    cut_off));


%% This finds the points where the average of slope is calculated

if ind_l(2)< (No_pt_slp+2) || ind_r(2)< (No_pt_slp+2)
    No_pt_slp = min(abs((ind_l(2)−1)),abs((ind_r(2)−1)));
end


x_avg_slope_l = zeros(No_ind,(2*No_pt_slp+1));
z_avg_slope_l = x_avg_slope_l;

for k = 2:No_ind
    ind_slope = (−No_pt_slp:1:+No_pt_slp)+ind_l(k);
    x_avg_slope_l(k,:) = x_l(ind_slope);
    z_avg_slope_l(k,:) = z_l(ind_slope);
end

x_avg_slope_r = zeros(No_ind,(2*No_pt_slp+1));
z_avg_slope_r = x_avg_slope_r;

for k = 2:No_ind
    ind_slope = (−No_pt_slp:1:+No_pt_slp)+ind_r(k);
    x_avg_slope_r(k,:) = x_r(ind_slope);
    z_avg_slope_r(k,:) = z_r(ind_slope);
end

%% Finds the average slope

avg_slope_l = zeros(No_ind,1);

if (2*No_pt_slp+1)−(2*dif_slp) == 0
    dif_slp = dif_slp −1;
elseif (2*No_pt_slp+1)−(2*dif_slp) == −1
    dif_slp = dif_slp −2;
end

for k = 2:No_ind
```

```
    slope_temp = zeros(1,((2*No_pt_slp+1)-(2*dif_slp)));
    for j = (dif_slp+1):(2*No_pt_slp+1)-dif_slp
                                        % slope carried bet 3 pts
        slope_temp(k,j-dif_slp) = (z_avg_slope_l(k,j+dif_slp)-
           z_avg_slope_l(k,j-dif_slp))/(x_avg_slope_l(k,j+dif_slp
           )-x_avg_slope_l(k,j-dif_slp));
    end
    avg_slope_l(k,1) = mean(slope_temp(k,:));
end

avg_slope_r = zeros(No_ind,1);

for k = 2:No_ind
    slope_temp = zeros(1,((2*No_pt_slp+1)-(2*dif_slp)));
    for j = (dif_slp+1):(2*No_pt_slp+1)-dif_slp
                                        % slope carried bet 3 pts
        slope_temp(k,j-dif_slp) = (z_avg_slope_r(k,j+dif_slp)-
           z_avg_slope_r(k,j-dif_slp))/(x_avg_slope_r(k,j+dif_slp
           )-x_avg_slope_r(k,j-dif_slp));
    end
    avg_slope_r(k,1) = mean(slope_temp(k,:));
end

%% check_l/r is used to vary the pixel direction

check_l = zeros(No_ind,1);

for k = 1:No_ind

    if avg_slope_l(k,1) ≥0 && avg_slope_l(k,1)≤ tan(22.5*pi/180)

        check_l(k) = 1;
    elseif  avg_slope_l(k,1) > tan(22.5*pi/180) && avg_slope_l(k
       ,1)≤ tan(67.5*pi/180)

        check_l(k) = 2;
    elseif avg_slope_l(k,1) > tan(67.5*pi/180) || avg_slope_l(k
       ,1)≤ tan(112.5*pi/180)

        check_l(k) = 3;
    elseif avg_slope_l(k,1) > tan(112.5*pi/180) && avg_slope_l(k
       ,1)≤ tan(157.5*pi/180)

        check_l(k) = 4;
    elseif avg_slope_l(k,1) > tan(157.5*pi/180) && avg_slope_l(k
       ,1) < 0

        check_l(k) = 5;
    end
```

```
end

check_r = zeros(No_ind,1);

for k = 1:No_ind

    if avg_slope_r(k,1) ≥0 && avg_slope_r(k,1)≤ tan(22.5*pi/180)

        check_r(k) = 1;
    elseif  avg_slope_r(k,1) > tan(22.5*pi/180) && avg_slope_r(k
       ,1)≤ tan(67.5*pi/180)

        check_r(k) = 2;
    elseif  avg_slope_r(k,1) > tan(67.5*pi/180) || avg_slope_r(k
       ,1)≤ tan(112.5*pi/180)

        check_r(k) = 3;
    elseif avg_slope_r(k,1) > tan(112.5*pi/180) && avg_slope_r(k
       ,1)≤ tan(157.5*pi/180)

        check_r(k) = 4;
    elseif avg_slope_r(k,1) > tan(157.5*pi/180) && avg_slope_r(k
       ,1) < 0

        check_r(k) = 5;
    end

end

%% Finds the Data points on drop profile

[ x_sub_l,z_sub_l ] = pixel_data(x_data_all,z_data_all,x_l,z_l,
   apex_x,apex_z,No_ind,No_pt_slp,ind_l,check_l,IC);
[ x_sub_r,z_sub_r ] = pixel_data(x_data_all,z_data_all,x_r,z_r,
   apex_x,apex_z,No_ind,No_pt_slp,ind_r,check_r,IC);

%%
x_abs_l = zeros(No_ind,1);
z_abs_l = x_abs_l;

x_plot_l = zeros(size(x_sub_l));
z_plot_l = x_plot_l;
x_plot_r = zeros(size(x_sub_r));
z_plot_r = x_plot_r;

for k = 1:No_ind
    [ x_abs_l(k,1),z_abs_l(k,1),x_plot,z_plot ] = abs_data_pts(
       x_sub_l(k,:),z_sub_l(k,:),k);
    x_plot_l(k,:) = x_plot;
    z_plot_l(k,:) = z_plot;
end

x_abs_r = zeros(No_ind,1);
z_abs_r = x_abs_r;

for k = 1:No_ind
    [ x_abs_r(k,1),z_abs_r(k,1),x_plot,z_plot ] = abs_data_pts(
       x_sub_r(k,:),z_sub_r(k,:),k);
    x_plot_r(k,:) = x_plot;
    z_plot_r(k,:) = z_plot;
end

%% Restructuring points

true_apex_x = x_abs_r(1);
true_apex_z = z_abs_r(1);

apex_diff_x = apex_x -  true_apex_x;
apex_diff_z = apex_z -  true_apex_z;

x_lhs = x_abs_l - true_apex_x;
z_lhs = z_abs_l - true_apex_z;

x_rhs = x_abs_r - true_apex_x;
z_rhs = z_abs_r - true_apex_z;


x_plot_l = x_plot_l - true_apex_x;
z_plot_l = z_plot_l - true_apex_z;
x_plot_r = x_plot_r - true_apex_x;
z_plot_r = z_plot_r - true_apex_z;

%%
xpl = xpl_i - true_apex_x;
zpl = zpl_i - true_apex_z;
xpr = xpr_i - true_apex_x;
zpr = zpr_i - true_apex_z;

%% clear

clear avg_slope_l avg_slopr_r check_l check_r cut_l cut_r dh_l
   dh_r
clear height_l height_r ind_l ind_r ind_slopr slope_temp
clear x_abs_l x_abs_r x_avg_slope_l x_avg_slope_r x_sub_l x_sub_r
clear z_abs_l z_abs_r z_avg_slope_l z_avg_slope_r z_sub_l z_sub_r

%% Scaling done here
```

```
[x_left_cm,z_left_cm, x_right_cm,z_right_cm,xl_cm,xr_cm,zl_cm,
   zr_cm  ] = scale_data(x_lhs,z_lhs,x_rhs,z_rhs,xpl,xpr,zpl,zpr,
   scale);


%%
p_l = polyfit(xl_cm,zl_cm,1);

p_r = polyfit(xr_cm,zr_cm,1);

p_l(1) = -p_l(1);

%% Find optimum 'b' 'c'

if d_side == 1
[b_l,c_l] = bc_optimization(-x_left_cm,z_left_cm,No_ind);
[b_r,c_r] = bc_optimization_la(x_right_cm,z_right_cm,No_ind);
elseif d_side == 2
[b_l,c_l] = bc_optimization_la(-x_left_cm,z_left_cm,No_ind);
[b_r,c_r] = bc_optimization(x_right_cm,z_right_cm,No_ind);
else
[b_l,c_l] = bc_optimization(-x_left_cm,z_left_cm,No_ind);
[b_r,c_r] = bc_optimization(x_right_cm,z_right_cm,No_ind);
end



%% finds theta
[x_ly_l,z_ly_l,theta_l,vol_l,Err_theta_l] = contact_angle(b_l,c_l
   ,p_l,S_span,scale);
[x_ly_r,z_ly_r,theta_r,vol_r,Err_theta_r] = contact_angle(b_r,c_r
   ,p_r,S_span,scale);

%% Finds drop volume and theta
drop_volume = (vol_l+vol_r)/2;
[ eq_radius,wet_radius,drop_height_l,drop_height_r] =
   drop_properties( x_ly_l,z_ly_l,x_ly_r,z_ly_r);

tilt_left  = atand(-p_l(1));
tilt_right = atand(p_r(1));
%%
xl_n = -x_ly_l*scale;
zl_n = z_ly_l*scale;
xr_n = x_ly_r*scale;
zr_n = z_ly_r*scale;

x_l_n = xl_n + true_apex_x;
z_l_n = zl_n + true_apex_z;
```

```
x_r_n = xr_n + true_apex_x;
z_r_n = zr_n + true_apex_z;

%%
p_l_i = polyfit(xpl_i,zpl_i,1);

p_r_i = polyfit(xpr_i,zpr_i,1);


x_new_l = linspace(1,(xpl_i(end)+80),500);
x_new_r = linspace((xpr_i(1)−80),xpr_i(end),500);

z_new_l = polyval(p_l_i,x_new_l);
z_new_r = polyval(p_r_i,x_new_r);


figure
imshow(IC);
hold on
plot(x_l_n,z_l_n,'g',x_r_n,z_r_n,'g');
plot(x_new_l,z_new_l,'c',x_new_r,z_new_r,'c')

imagenumber = file(1:end−4);
imagefolder = [folder,'Images\',imagenumber,'_drop','.fig'];
saveas(gcf,imagefolder)
clear gcf
close all

%% Plots LY profile
figure
for k = 1:No_ind
    hold on
    plot(x_plot_l(k,:)/scale,z_plot_l(k,:)/scale,'r');
    plot(x_plot_r(k,:)/scale,z_plot_r(k,:)/scale,'r');
end


plot((−x_ly_l),z_ly_l,'b',x_ly_r,z_ly_r,'b')
set(gca,'YDir','reverse');
axis([−.5 .5 −.5 .5]);
axis square

% Saves the figure
imagenumber = file(1:end−4);
imagefolder = [folder,'Images\',imagenumber,'.fig'];
saveas(gcf,imagefolder)
clear gcf
close all
```

```
    %% Solution stored in the m file
        Data(r,:) = [ eq_radius wet_radius drop_height_l
           drop_height_r c_l c_r b_l b_r drop_volume tilt_left
           tilt_right theta_l theta_r];
        Err_data(r,:) = cat(1,Err_theta_l,Err_theta_r);
        No_pt_slp = 16;         % No of pts used for quadratic fit on
           each side
        dif_slp   = 3;
end

%% Saves the result
datafolder = [folder,'Data\','Data'];
errfolder  = [folder,'Data\','Err_data'];
strutfolder  = [folder,'Data\','Struct_A'];
save(datafolder,'Data')
save(errfolder,'Err_data')
save(strutfolder,'A')
```

2.4 Functions

Here is a list of all of the functions used in the contact angle measurement program in alphabetical order.

2.4.1 abs_data_pts

```
function [ x_abs,z_abs,xx,pp ] = abs_data_pts(x,z,iter)
% This function fits a quadratic curve between the points and
% finds optimum point.

fit = 2;                    % Fit types
n = length(x);

if iter == 1

    xx = x(1):((x(end)-x(1))/(n*50)):x(end);
    p = polyfit(x,z,fit);
    pp = polyval(p,xx);

    z_abs = min(pp);
    x_abs = xx(find(pp == z_abs)); %#ok<FNDSB>

    xx = x;
    pp = polyval(p,xx);
else

    dx = diff(x);

    if any(dx<=0)
        zz = z(1):((z(end)-z(1))/(n-1)):z(end);
        p = polyfit(z,x,fit);
        pp = polyval(p,zz);

        x_abs = pp((n+1)/2);
        z_abs = zz((n+1)/2);

        xx = pp;
        pp = zz;
    else
        xx = x(1):((x(end)-x(1))/(n-1)):x(end);
        p = polyfit(x,z,fit);
        pp = polyval(p,xx);

        x_abs = xx((n+1)/2);
        z_abs = pp((n+1)/2);
    end

end

end

%eof
```

2.4.2 bc_optimization

```
function [b_opt,c_opt] = bc_optimization(x_n,z_n,N)

S_span=(0:.001:6); % S_span is the step variable for ode45 solver
step_i = 0.1;

%%
c = 13.45;
[b_initial] = Initial_guess(x_n,z_n,c,N);
Bini = b_initial*(c^.5) ;

if Bini ≤ .2005
    step_i = (Bini-0.005)/2;
end

Bnew = [(Bini-2*step_i) (Bini-step_i) (Bini) (Bini+step_i) (Bini+2*
    step_i)];
C = zeros(1,5);
err = zeros(1,5);

for j = 1:length(Bnew);
    [ C(j),err(j) ] = cfinder(Bnew(j),c,x_n,z_n,N,S_span );
end

ind = find(min(abs(err))==abs(err));

Cnew = zeros(1,5);
errnew = Cnew;

%%

while (step_i)>0.0001

    if ind == 1
```

```
        Bnew1 = [(Bini-6*step_i) (Bini-5*step_i) (Bini-4*step_i) (
           Bini-3*step_i) (Bini-2*step_i)];
        Cnew(5) = C(1);
        errnew(5) = err(1);

        condn = 1;
    elseif ind == 5
        Bnew1 = [(Bini+2*step_i) (Bini+3*step_i) (Bini+4*step_i) (
           Bini+5*step_i) (Bini+6*step_i)];
        condn = 2;
        Cnew(1) = C(5);
        errnew(1) = err(5);

    else
        Bnew1 = [(Bnew(ind)-step_i) (Bnew(ind)-.5*step_i) (Bnew(ind))
            (Bnew(ind)+.5*step_i) (Bnew(ind)+step_i)];
        condn = 3;
        Cnew(1) = C(ind-1);
        Cnew(3) = C(ind);
        Cnew(5) = C(ind+1);
        errnew(1) = err(ind-1);
        errnew(3) = err(ind);
        errnew(5) = err(ind+1);
    end

    %%

    if condn == 1
        for j = 1:4
            [ Cnew(j),errnew(j) ] = cfinder(Bnew1(j),c,x_n,z_n,N,
               S_span );
        end
    elseif condn ==2
        for j = 2:5
            [ Cnew(j),errnew(j) ] = cfinder(Bnew1(j),c,x_n,z_n,N,
               S_span );
        end
    elseif condn == 3
        for j = [2,4]
            [ Cnew(j),errnew(j) ] = cfinder(Bnew1(j),c,x_n,z_n,N,
               S_span );
        end
    end

    ind = find(min(abs(errnew))==abs(errnew));

    if length(ind)>1
        ind = round(mean(ind));
    end
```

```
        C = Cnew;
        err = errnew;
        step_i = step_i/2;

        Bini = Bnew1(3);
        Bnew = Bnew1;

    end

    c_opt = Cnew(ind);
    B_opt = Bnew1(ind);
    b_opt = B_opt/(c_opt^.5);

end

% eof
```

2.4.3 bc_optimization_la

```
function [b_opt,c_opt] = bc_optimization_la(x_n,z_n,N)
% Optimization with low accuracy for faster processing

S_span=(0:.001:6); % S_span is the step variable for ode45 solver
step_i = 0.1;

%%

c = 13.45;
[b_initial] = Initial_guess(x_n,z_n,c,N);

Bini = b_initial*(c^.5) ;

if Bini <= .2005
    step_i = (Bini-0.005)/2;
end

Bnew = [(Bini-2*step_i) (Bini-step_i) (Bini) (Bini+step_i) (Bini+2*
    step_i)];

C = zeros(1,5);
err = zeros(1,5);

for j = 1:length(Bnew);
```

```
    [ C(j),err(j) ] = cfinder(Bnew(j),c,x_n,z_n,N,S_span );
end

ind = find(min(abs(err))==abs(err));

Cnew = zeros(1,5);
errnew = Cnew;

%%

while (step_i)>0.005


    if ind == 1
        Bnew1 = [(Bini-6*step_i) (Bini-5*step_i) (Bini-4*step_i) (
           Bini-3*step_i) (Bini-2*step_i)];
        Cnew(5) = C(1);
        errnew(5) = err(1);

        condn = 1;
    elseif ind == 5
        Bnew1 = [(Bini+2*step_i) (Bini+3*step_i) (Bini+4*step_i) (
           Bini+5*step_i) (Bini+6*step_i)];
        condn = 2;
        Cnew(1) = C(5);
        errnew(1) = err(5);

    else
        Bnew1 = [(Bnew(ind)-step_i) (Bnew(ind)-.5*step_i) (Bnew(ind))
             (Bnew(ind)+.5*step_i) (Bnew(ind)+step_i)];
        condn = 3;
        Cnew(1) = C(ind-1);
        Cnew(3) = C(ind);
        Cnew(5) = C(ind+1);
        errnew(1) = err(ind-1);
        errnew(3) = err(ind);
        errnew(5) = err(ind+1);

    end

    %%

    if condn == 1
        for j = 1:4
            [ Cnew(j),errnew(j) ] = cfinder(Bnew1(j),c,x_n,z_n,N,
               S_span );
        end
    elseif condn ==2
        for j = 2:5
```

```
            [ Cnew(j),errnew(j) ] = cfinder(Bnew1(j),c,x_n,z_n,N,
               S_span );
        end
    elseif condn == 3
        for j = [2,4]
            [ Cnew(j),errnew(j) ] = cfinder(Bnew1(j),c,x_n,z_n,N,
               S_span );
        end
    end

    %% % % % % % % % % % %

    ind = find(min(abs(errnew))==abs(errnew));

    if length(ind)>1
        ind = round(mean(ind));
    end

    C = Cnew;
    err = errnew;
    step_i = step_i/2;

    Bini = Bnew1(3);
    Bnew = Bnew1;

end

%%
c_opt = Cnew(ind);
B_opt = Bnew1(ind);
b_opt = B_opt/(c_opt^.5);


end

% eof
```

2.4.4 cfinder

```
function [ C,err ] = cfinder(Bini,c,x_n,z_n,N,S_span )
% This function finds the optimum `c' for given B

b = Bini/(c^.5);

```

```
[S,Y] = ode45(@laplace,S_span,[0 1e-100 0],[],b,c); % may need to
   increase second input if curve does not loop

Z=Y(:,1);

i=1;
while Z(i)<Z(i+1);      % finds where contact angle is 180 degrees (
   cutoff point)
    i=i+1;
end;

x_ly(1:i,1)=Y(1:i,2);            % Drop height dimensionless
z_ly(1:i,1)=Y(1:i,1);            % Drop x dimension dimensionless

clear S_ly S Z Y x_ly_or_c z_ly_or_c

%%

iter = 1;
c1 = 10;
c2 = 20;

x_lynew = x_ly/(c1^.5);
z_lynew = z_ly/(c1^.5);
[error_profile1] = error_drop_new_w_sign(x_n,z_n,x_lynew,z_lynew,N );
clear x_lynew z_lynew

x_lynew = x_ly/(c2^.5);
z_lynew = z_ly/(c2^.5);
[error_profile2] = error_drop_new_w_sign(x_n,z_n,x_lynew,z_lynew,N );
     %#ok<NASGU>
clear x_lynew z_lynew

close all
while iter ≤16
    c3 = (c1+c2)/2;
    x_lynew = x_ly/(c3^.5);
    z_lynew = z_ly/(c3^.5);
    [error_profile] = error_drop_new_w_sign(x_n,z_n,x_lynew,z_lynew,N
        );
    clear x_lynew z_lynew

    if error_profile*error_profile1<0
        c2 = c3;
        error_profile2 = error_profile; %#ok<NASGU>
    else
        c1 = c3;
        error_profile1 = error_profile;
    end
    iter = iter+1;
end
C = c3;
err =abs( error_profile);
clear x_ly z_ly S Z Y

end

% eof
```

2.4.5 cfinder_la

```
function [ C,err ] = cfinder_la(Bini,c,x_n,z_n,N,S_span )
%UNTITLED2 Summary of this function goes here
%   Detailed explanation goes here

b = Bini/(c^.5);


[S,Y] = ode45(@laplace,S_span,[0 1e-100 0],[],b,c); % may need to
   increase second input if curve does not loop

Z=Y(:,1);

i=1;
while Z(i)<Z(i+1); % finds where contact angle is 180 degrees (cutoff
    point)
    i=i+1;
end;

x_ly(1:i,1)=Y(1:i,2);%/(c^.5);            % Drop height dimensionless
z_ly(1:i,1)=Y(1:i,1);%/(c^.5);            % Drop x dimension
   dimensionless


clear S_ly S Z Y x_ly_or_c z_ly_or_c



%%
iter = 1;
c1 = 10;
c2 = 19;
```

```

x_lynew = x_ly/(c1^.5);
z_lynew = z_ly/(c1^.5);
[error_profile1] = error_drop_new_w_sign(x_n,z_n,x_lynew,z_lynew,N );
clear x_lynew z_lynew


x_lynew = x_ly/(c2^.5);
z_lynew = z_ly/(c2^.5);
[error_profile2] = error_drop_new_w_sign(x_n,z_n,x_lynew,z_lynew,N );
    %#ok<NASGU>
clear x_lynew z_lynew


close all
while iter ≤9
    c3 = (c1+c2)/2;
    x_lynew = x_ly/(c3^.5);
    z_lynew = z_ly/(c3^.5);
    [error_profile] = error_drop_new_w_sign(x_n,z_n,x_lynew,z_lynew,N
        );
    clear x_lynew z_lynew
    if error_profile*error_profile1<0
        c2 = c3;
        error_profile2 = error_profile; %#ok<NASGU>
    else
        c1 = c3;
        error_profile1 = error_profile;
    end

    %         atr(iter) = error_profile;
    iter = iter+1;
end
C = c3;
err =abs( error_profile);
%     close all

clear x_ly z_ly S Z Y





end
```

2.4.6 contact_angle

```
function [x_ly_profile,z_ly_profile,theta,drop_vol,Err_t] =
   contact_angle(b,c,p,S_span,scale )
% This function finds the final contact angle

[S,Y] = ode45(@laplace,S_span,[0 1e−100 0],[],b,c); % may need to
   increase second input if curve does not loop
Z = Y(:,1);

i = 1;
while Z(i)<Z(i+1); % finds where contact angle is 180 degrees (cutoff
    point)
    i = i+1;
end

x_ly = zeros(i,1);
z_ly = zeros(i,1);

x_ly(1:i,1)=Y(1:i,2)/(c^.5);            % Drop height dimensionless
z_ly(1:i,1)=Y(1:i,1)/(c^.5);            % Drop x dimension
   dimensionless

j = 1;

while(z_ly(j) ≤ (p(1)*x_ly(j)+p(2)))&& j<(i−10) ;
    j = j+1;
end

ind_end = j;
x_ly_profile = x_ly(1:ind_end);
z_ly_profile = z_ly(1:ind_end);

angle = Y(ind_end,3)*180/pi;   % Angle

theta = angle;

drop_vol = volume(z_ly,x_ly,z_ly_profile(end));

drop_height = z_ly_profile(end);

%%
Err_t = zeros(1,51);        % Error matrix for interface correction
for j = −25:1:25
    Err_t(1,j) = Y(find(z_ly ≤ drop_height+j/scale,1,'last'));
end
```

```
end

% eof
```

2.4.7 drop_properties

```
function [ eq_rad,wet_rad,drop_ht_l,drop_ht_r] = drop_properties( x_l
    ,z_l,x_r,z_r)
% Finds physical drop properties

eq_rad = (max(abs(x_l)) + max(abs(x_r)))/2;
wet_rad = (abs(x_l(end) + abs(x_r(end))))/2;

drop_ht_l = z_l(end);
drop_ht_r = z_r(end);

end

% eof
```

2.4.8 edge_detector

```
function [flip_bound]=edge_detector(Black_White)
% This function  converts the image into grayscale
% from Russell Stacy (2009)

boundary_full = bwtraceboundary(Black_White,[1,1],'S');  % Find total
     boundary of image

bound1 = boundary_full(find(boundary_full(:,2)==(length(Black_White
    (1,:))-1), 1, 'last' ):length(boundary_full(:,1))-max(
    boundary_full(:,1)),1); % trim the full boundary of column one to
    eliminate the image edge

bound2 = boundary_full(find(boundary_full(:,2)==(length(Black_White
    (1,:))-1), 1, 'last' ):length(boundary_full(:,1))-max(
    boundary_full(:,1)),2); % trim the full boundary of column two to
    eliminate the image edge

```

```
bound = [bound2,bound1];    % Recombine the two colums to form a
    vector of values [x,y]
flip_bound = flipud(bound); % The "bound" vector is in reverse order
    of data points from right to left. flipud() flips the vectors to
    follow data points from left to right

end

% eof
```

2.4.9 error

```
function [error_profile] = error_drop(x_cm,z_cm,x_ly,z_ly,N )
% Finds the error in the drop profile

nop = 200;                    %Number fo points for fit
N_ly = length(x_ly);
distance1 = zeros(N_ly,1);
distance2 = zeros(nop,1);
distance_min = zeros(N,1);
distance_min_sign = zeros(N,1);

%%
weigh = 1;% sqrt(1:1:N);

for j = 2:N

    for k = 1:N_ly
        distance1(k,1) = sqrt( (x_cm(j)-x_ly(k))^2 + (z_cm(j)-z_ly(k)
            )^2 );
    end

    ind_z = find(min(distance1)==distance1);

    if ind_z == N_ly;
        ind_z = ind_z-2;
    end

    ind = (ind_z-2):1:(ind_z+2);
    p = polyfit(x_ly(ind),z_ly(ind),2);

    x_cut = linspace(x_ly(ind(1)),x_ly(ind(end)),nop);
    z_cut = polyval(p,x_cut);

    for k = 1:nop
```

```
        distance2(k) = sqrt((x_cut(k)-x_cm(j))^2+(z_cut(k)-z_cm(j))
           ^2);
    end

    ind_min = find(min(distance2)==distance2);

    if x_cm(j) < x_cut(ind_min)
        sign_error = 1;
    else
        sign_error = -1;
    end

    distance_min(j,1) = min(distance2)*weigh;
    distance_min_sign(j,1) = sign_error*min(distance2)*weigh;

end
error_profile = sum(distance_min)*(abs(sum(distance_min_sign))/sum(
   distance_min_sign));

end

% eof
```

2.4.10 exact_data

```
function [ x,z ] = exact_data(x_fit,z_fit,check,pixel_index)
% Based on input value of check, this function gives exact profile
   data;

n_pts = length(x_fit);

if check == 1 || check == 5

    base_pts_z = linspace(z_fit(1),z_fit(end),(n_pts*100)+1);
    spline_fit_z = spline(z_fit,pixel_index,base_pts_z);

    median_up_z = median(pixel_index(1:5));
    median_dn_z = median(pixel_index((end-5):end));

    intensity_z = (median_up_z+median_dn_z)/2;
    dif_z = abs(intensity_z-spline_fit_z);

    x = mean(x_fit);
    z = base_pts_z(find(dif_z == min(dif_z),1,'first'));
```

```
elseif check == 2 || check == 4

    base_pts_x = linspace(x_fit(1),x_fit(end),(n_pts*100)+1);
    base_pts_z = linspace(z_fit(1),z_fit(end),(n_pts*100)+1);

    spline_fit_x = spline(x_fit,pixel_index,base_pts_x);

    median_up_x = median(pixel_index(1:5));
    median_dn_x = median(pixel_index((end-5):end));

    intensity_x = (median_up_x+median_dn_x)/2;
    dif_x = abs(intensity_x-spline_fit_x);

    x = base_pts_x(find(dif_x == min(dif_x),1,'first'));
    z = base_pts_z(find(dif_x == min(dif_x),1,'first'));

elseif check == 3

    base_pts_x = linspace(x_fit(1),x_fit(end),(n_pts*100)+1);
    spline_fit_x = spline(x_fit,pixel_index,base_pts_x);

    median_up_x = median(pixel_index(1:5));
    median_dn_x = median(pixel_index((end-5):end));

    intensity_x = (median_up_x+median_dn_x)/2;
    dif_x = abs(intensity_x-spline_fit_x);

    x = base_pts_x(find(dif_x == min(dif_x),1,'first'));
    z = mean(z_fit);

end

end

% eof
```

2.4.11 image_analysis

```
function [Black_White,Trimmed_image]=image_analysis(Cropped_Image)
% This funtion produces the black and white image

co=10; % co is cutoff for top and bottom and left and right of image

```

```
thresh=0.85;

BW1=im2bw(Cropped_Image,thresh); % thresh is the threshold of the
   image for converting to black and white.

Trimmed_image=Cropped_Image(co:length(Cropped_Image(:,1))−co,co:
   length(Cropped_Image(1,:))−co);
Black_White=BW1(co:length(BW1(:,1))−co,co:length(BW1(1,:))−co);

end

% eof
```

2.4.12 image_input

```
function [Drop_Image,filepath,filename]=image_input(im_no,ex_type,
   prefix_img,start_no,range_lim,filepath)
% This function reads the images

image_no = start_no+im_no−1;      % Image number
image_names = num2str(image_no);  % Image number in string

if ex_type == 2              % Adds 0s if required
    if range_lim == 3
        if image_no <10
            image_names = ['0','0',image_names];
        elseif image_no ≥10 && image_no <100
            image_names = ['0',image_names];
        end
    elseif range_lim == 2
        if image_no <10
            image_names = ['0',image_names];
        end
    end
end

filename = [prefix_img,image_names,'.tif'];  % Image name
Drop_Image = imread([filepath,filename]);    % Image read

end

% eof
```

2.4.13 initial_guess

```
function [b_initial] = Initial_guess(x_n,z_n,c,N)
% Initial guess. Extracted from Russell Stacy (2009)

S_span = 0:.002:5;
up = N-5;

%%
iter = 1;
b1=3;
b2=.01;

bb=[b1 b2];            % range of b values to use

for j=1:2;

    b=bb(j);             % set b as individual values of b

    [S,Y] = ode45(@laplace,S_span,[0 1e-100 0],[],b,c);
    Z=Y(:,1);

    i=1;
    while Z(i)<Z(i+1);
        i=i+1;
    end;
    x_ly(1:i,j)=Y(1:i,2)/(c^.5);
    z_ly(1:i,j)=Y(1:i,1)/(c^.5);

end;

%% Error

[d1,z1]=min(abs(z_n(N-up)-z_ly(:,1))); % find indice of laplace data
   that closely matches raw data
error_b1=x_n(N-up)-x_ly(z1,1);         % finds relative horizontal
   error of end of trim data

[d2,z2]=min(abs(z_n(N-up)-z_ly(:,2))); % find indice of laplace data
   that closely matches raw data
error_b2=x_n(N-up)-x_ly(z2,2);         % finds relative horizontal
   error of end of trim data

if error_b1*error_b2>0 && error_b1<0;
    fprintf('choose smaller b2 value');
elseif error_b1*error_b2>0 && error_b1>0;
    fprintf('choose larger b1 value');
    return
end;

error_b=min(abs([error_b1 error_b2]));

%% Minimization

c_change=.1;
b=(b1+b2)/2;

b3=b;
while (iter≤20);
    clear x_ly z_ly S_ly Phi_ly Z

    [S,Y] = ode45(@laplace,S_span,[0 1e−100 0],[],b3,c); % may need
       to increase span of S if curve does not loop
    Z=Y(:,1); % the first column of Y is the Z data. Needs to be
       defined to find cutoff point below.

    i=1;
    while Z(i)<Z(i+1); % finds where contact angle is 180 degrees (
       cutoff point)
        i=i+1;
    end;

    % Output Variables

    x_ly_1(1:i)=Y(1:i,2)/(c^.5);             % Drop height
       dimensionless
    z_ly_1(1:i)=Y(1:i,1)/(c^.5);             % Drop width
       dimensionless

    [d3,z3]=min(abs(z_n(N−up)−z_ly_1)); % find indice of laplace data
        that closely matches raw data
    error_b3=x_n(N−up)−x_ly_1(z3);      % finds relative horizontal
       error of end of trim data

    if error_b3*error_b1>0;
        b1=b3;
        error_b1=error_b3;
        error_b=error_b1;
    else
        b2=b3;
        error_b2=error_b3;
        error_b=error_b2;
    end;
    b=b3;
    b3=(b1+b2)/2;
    iter = iter+1;
```

```
end;

b_initial = b3;

end
```

2.4.14 laplace

```
%Derek Fultz and Russ Stacy
%7-24-07
%
% LAPLACE defines the ordinary differential equations to be solved.
% z=drop height
% x=distance from axis to drop interface
% phi=contact angle
% 1/b=radius of curvature at apex
% s=arc length
%
% NON-DIMENSIONALIZE Z,X,S,B USING C^(1/2)
% B=b*c^(1/2)
% X=x*c^(1/2)
% Z=z*c^(1/2)
% S=s*c^(1/2)
%
% No need to define X,Z,S for equations
%
% KEY OF VARIABLE DEFINITIONS FOR SYSTEM
% Z=y(1); Z'=dy(1); Z' is with respect to S
% X=y(2); X'=dy(2); X' is with respect to S
% phi=y(3); phi'=dy(3); phi' is with respect to S
%
% Z'=sin(phi)
% X'=cos(phi)
% phi'=2/B+Z-(sin(phi)/X)

function [dy]=laplace(s,y,m,n)
dy = zeros(3,1); % a column vector

B=m*n^.5;         % non-dimensionalized curvature at apex

dy(1)=sin(y(3));
dy(2)=cos(y(3));
dy(3)=(2/B)+y(1)-(sin(y(3))/y(2));
```

```
end

% eof
```

2.4.15 plane

```
function [mean_left,mean_right,x_plane_left,x_plane_right,
    z_plane_left,z_plane_right ] = plane( I,boundary )
% This function finds the Solid—Liquid Interface

ini_z = boundary(:,2);

z_left_temp = ini_z(1:10);          % 10 pixels from left edge of
    image
z_right_temp = ini_z(end—10:end);   % 10 pixels from left edge of
    image

plane_left_ini  = round(mean(z_left_temp));  % Mean of left plane
plane_right_ini = round(mean(z_right_temp)); % Mean of right plane

apex_z_ind = (find(boundary(:,2)== min(boundary(:,2)),1,'first'));

x_left = boundary(1:apex_z_ind,1);
z_left = boundary(1:apex_z_ind,2);

x_right = boundary((apex_z_ind+1):end,1);
z_right = boundary((apex_z_ind+1):end,2);

cutoff_x_l = x_left(find(z_left == (plane_left_ini — 20),1,'last'));
cutoff_x_r = x_right(find(z_right == (plane_right_ini — 20),1,'first'
    ));

z_left_int  = I((plane_left_ini—18):(plane_left_ini+18),1:cutoff_x_l)
    ;
z_right_int = I((plane_right_ini—18):(plane_right_ini+18),cutoff_x_r:
    end);

z_left_img  = double(z_left_int);
z_right_img = double(z_right_int);

%%

for j = 1:length(z_left_img(1,:))
    for i = 1:(length(z_left_img(:,1))—4)
```

```
        dz_left(i,j)  = (z_left_img(i,j)−8*z_left_img(i+1,j)+8*
           z_left_img(i+3,j)−z_left_img(i+4,j))/12;
    end
end

for j = 1:length(z_right_img(1,:))
    for i = 1:(length(z_right_img(:,1))−4)
        dz_right(i,j)  = (z_right_img(i,j)−8*z_right_img(i+1,j)+8*
           z_right_img(i+3,j)−z_right_img(i+4,j))/12;
    end
end

%%

for j = 1:length(z_left_img(1,:))
    plane_left(j) = round(mean(find(abs(dz_left(:,j)) == max(abs(
       dz_left(:,j))) )));
end

for j = 1:length(z_right_img(1,:))
    plane_right(j) = round(mean(find(abs(dz_right(:,j)) == max(abs(
       dz_right(:,j))) )));
end

%%

z_plane_left  = plane_left + plane_left_ini−17;
z_plane_right = plane_right + plane_right_ini−17;

%%

I1 = I;
for j = 1:length(z_left_img(1,:));
    I1(round(z_plane_left(j)),j)=255;
end

for j = 1:length(z_right_img(1,:));
    k = cutoff_x_r + j −1;
    I1(round(z_plane_right(j)),k)=226;
end

mean_left = round(mean(z_plane_left));
mean_right = round(mean(z_plane_right));

%%

p_l = polyfit(1:length(z_plane_left),z_plane_left,1);
p_r = polyfit(cutoff_x_r:length(I(1,:)),z_plane_right,1);
```

```
%%

x_plane_left = 1:length(z_plane_left);
x_plane_right = cutoff_x_r:length(I(1,:));

end

% eof
```

2.4.16 pixel_data

```
function [ x_sub,z_sub ] = pixel_data(x_all,z_all,x_pts,z_pts,apex_x,
    apex_z,N,N_op,ind,check_xy,crop_im )
% This function gives the sub-pixel data for N_op points

x_mat = zeros(N,(2*N_op+1));                    % here  21 pts of x are
    stored (-10:10) for N points
z_mat = x_mat;

x_sub = x_mat;                                  % here  exact 21 pts of
    x are stored (-10:10) for N points
z_sub = z_mat;

%%

for j = 1:N
    if j == 1
        apex_indice = round((find(z_all == 0,1,'first')+find(z_all ==
            0,1,'last'))/2);
        ind_pts = (-N_op:1:N_op) + apex_indice;
        x_mat(1,:) = x_all(ind_pts);
        z_mat(1,:) = z_all(ind_pts);
    else
    ind_pts = (-N_op:1:N_op) + ind(j);
    x_mat(j,:) = x_pts(ind_pts);
    z_mat(j,:) = z_pts(ind_pts);
    end
end

x_mat = x_mat+apex_x;                        % apex added to make
    compatible with image
z_mat = z_mat+apex_z;
```

```
pix_ind = 15;                               % no of points taken in
    image for spline fit
pixel_index = zeros(1,(pix_ind));           % stores pixel data

for j = 1:N
    check = check_xy(j);
    if check == 1
        pix_ind_z = -7:1:7;
        for k = 1:(2*N_op+1)
            pix_x(1,1:(pix_ind)) = x_mat(j,k);
            pix_z = z_mat(j,k) + pix_ind_z;
            for m = 1:(pix_ind)
                pixel_index(1,m) = double(crop_im(pix_z(m),pix_x(m)))
                    ;
            end
            [x_sub(j,k),z_sub(j,k)] = exact_data(pix_x,pix_z,check,
               pixel_index);
        end

    elseif check == 2

        pix_ind_x = -7:1:7;
        pix_ind_z = 7:-1:-7;

        for k = 1:(2*N_op+1)

            pix_x = x_mat(j,k)+ pix_ind_x;
            pix_z = z_mat(j,k)+ pix_ind_z;

            for m = 1:(pix_ind)
                pixel_index(1,m) = double(crop_im(pix_z(m),pix_x(m)))
                    ;
            end
            [x_sub(j,k),z_sub(j,k)] = exact_data(pix_x,pix_z,check,
               pixel_index);

        end

    elseif check == 3

        pix_ind_x = -7:1:7;

        for k = 1:(2*N_op+1)

            pix_x(1,1:length(pix_ind_x)) = x_mat(j,k) + pix_ind_x;
            pix_z(1,1:length(pix_ind_x)) = z_mat(j,k);

            for m = 1:(pix_ind)
```

```
                pixel_index(1,m) = double(crop_im(pix_z(m),pix_x(m)))
                    ;
            end

            [x_sub(j,k),z_sub(j,k)] = exact_data(pix_x,pix_z,check,
               pixel_index);
        end

    elseif check == 4

        pix_ind_x = -7:1:7;
        pix_ind_z = -7:1:7;

        for k = 1:(2*N_op+1)

            pix_x(1,1:length(pix_ind_x)) = x_mat(j,k)+ pix_ind_x;
            pix_z(1,1:length(pix_ind_z)) = z_mat(j,k)+ pix_ind_z;

            for m = 1:(pix_ind)
                pixel_index(1,m) = double(crop_im(pix_z(m),pix_x(m)))
                    ;
            end
            [x_sub(j,k),z_sub(j,k)] = exact_data(pix_x,pix_z,check,
               pixel_index);
        end

    elseif check == 5

        pix_ind_z = -7:1:7;

        for k = 1:(2*N_op+1)

            pix_x(1,1:length(pix_ind_z)) = x_mat(j,k);
            pix_z(1,1:length(pix_ind_z)) = z_mat(j,k) + pix_ind_z;

            for m = 1:(pix_ind)
                pixel_index(1,m) = double(crop_im(pix_z(m),pix_x(m)))
                    ;
            end

            [x_sub(j,k),z_sub(j,k)] = exact_data(pix_x,pix_z,check,
               pixel_index);
        end

    end

end

end
```

```
%eof
```

2.4.17 profile_split

```
function [x_data_all,z_data_all,x_l,z_l,x_r,z_r,apex_x,apex_z] =
    profile_split( boundary,mean_l,mean_r)
%%
apex_z = min(boundary(:,2));                                  %
    Gives z position of apex
apex_x = boundary(round(mean(find(boundary(:,2) == apex_z))),1); %
    Gives x position of apex

x_data_all = boundary(:,1) - apex_x;     %  all x data
z_data_all = boundary(:,2) - apex_z;     %  all z data

apex_ind = round((find(z_data_all == 0,1,'first')+find(z_data_all ==
    0,1,'last'))/2);

z_left = z_data_all(1:apex_ind);
z_right = z_data_all((apex_ind+1):end);

z_cut_l = find(z_left == ((mean_l-20)-apex_z),1,'last');
z_cut_r = find(z_right == ((mean_r-20)-apex_z),1,'first')+apex_ind;

x_data = x_data_all(z_cut_l:z_cut_r);
z_data = z_data_all(z_cut_l:z_cut_r);

apex_ind_n = round((find(z_data == 0,1,'first')+find(z_data == 0,1,'
    last'))/2);

x_l = x_data(apex_ind_n:-1:1);      % Note apex is the start and the
    end point
z_l = z_data(apex_ind_n:-1:1);

x_r = x_data(apex_ind_n:end);
z_r = z_data(apex_ind_n:end);

end
```

2.4.18 scale_data

```
function [x_left_cm,z_left_cm, x_right_cm,z_right_cm,xl_cm,xr_cm,
    zl_cm,zr_cm  ] = scale_data(x_left,z_left,x_right,z_right,xpl,xpr,
    zpl,zpr,scale)
% Scale the data

x_left_cm = x_left/scale;
z_left_cm = z_left/scale;

x_right_cm = x_right/scale;
z_right_cm = z_right/scale;

xl_cm = xpl/scale;
xr_cm = xpr/scale;
zl_cm = zpl/scale;
zr_cm = zpr/scale;

end

% eof
```

2.4.19 volume

```
function [drop_vol] = volume(z_ly_1,x_ly_1,drop_height_nd)
% This function finds the volume using washers scheme

Z_ly_ind = find(z_ly_1 ≤ drop_height_nd);  % Index of end point on
    drop

Z_ly = z_ly_1(1:length(Z_ly_ind));           % End Z
X_ly = x_ly_1(1:length(Z_ly_ind));           % End X

V = zeros(length(Z_ly)−1,1);                  % Size of Volume matrix

for n = 2:length(Z_ly)
    V(n−1) = pi*(((X_ly(n)+X_ly(n−1))/2)^2)*(Z_ly(n)−Z_ly(n−1));
end

drop_vol = sum(V)*1000;

end

% eof
```

2.5 images_reader

```
%% This program load the 'xxx_drop.fig' files to check for error

clear
clc

mult = 1;
image_no =  1;   % Start image no
end_no = 100;    % End image no

k = 0;
j = 1;

step_size = 1;

filepath =  'C:\ABCD\ABCD\Images\';

Image = image_no;

while image_no ≤ end_no

    image_names = num2str(image_no);

    if image_no <10
        image_names = ['0','0',image_names];
    elseif image_no ≥10 && image_no <100
        image_names = ['0',image_names];
    end

    filename = ['A',image_names,'_drop','.fig'];

    open([filepath,filename]);

        l = input('');
        if isempty(l)
            Correction(j,1) = 0;
        else
            Correction(j,1) = l;
        end

        r = input('');
        if isempty(r)
            Correction(j,2) = 0;
        else
            Correction(j,2) = r;
        end
    close gcf

    if step_size == 1
    j = j+1;
    image_no = image_no+mult*step_size;
    elseif step_size == 2
        Correction(j+1,:) = Correction(j,:);
        j = j+2;
        image_no = image_no+mult*step_size;
    elseif step_size == 3
        Correction(j+1,:) = Correction(j,:);
        Correction(j+2,:) = Correction(j,:);
        j = j+3;
        image_no = image_no+mult*step_size;
    elseif step_size == 4
        Correction(j+1,:) = Correction(j,:);
        Correction(j+2,:) = Correction(j,:);
        Correction(j+3,:) = Correction(j,:);
        j = j+4;
        image_no = image_no+mult*step_size;
    end

    Image(j) = image_no;
end


save('C:\ABCD\ABCD\Data\Correction.mat','Correction')

% eof
```

2.6 Data_modifier

```
% Loads and does all the modifications

clc
clear
filepath = 'C:\ABCD\ABCD\';

mid1 = 26;

mid2 = 77;
%%
Data_file = [filepath,'Data\','Data.mat'];
Corr_file = [filepath,'Data\','Correction.mat'];
Err_file  = [filepath,'Data\','Err_data.mat'];

D1 = load(Data_file);
C1 = load(Corr_file);
E1 = load(Err_file);

Vol = D1.Data(:,9,1);
Error_Data = E1.Err_data(:,:,1);

%%

Theta_l = D1.Data(:,12,1);
Theta_r = D1.Data(:,13,1);

plot(Vol,Theta_l,'ro',Vol,Theta_r,'bo')
legend('Left','Right')

Corr_l_1 = C1.Correction(:,1,1);
Corr_r_1 = C1.Correction(:,2,1);

%%

if length(Theta_l) ≠ length(Corr_l_1)
    fprintf('Dimensions of Corr1 mismatch')
    Corr_l_1 = C1.Correction(1:length(Theta_l),1,1);
    Corr_r_1 = C1.Correction(1:length(Theta_r),2,1);
end

%%

Correction_l = Corr_l_1;
Correction_r = Corr_r_1;
```

```
%%

for j = 1:length(Vol)
    if Correction_r(j) == 0
        Theta_r_mod(j,1) = Theta_r(j);

    elseif round(Correction_r(j)) ≠ Correction_r(j)
        adder = (Correction_r(j)−floor(Correction_r(j)))*(Error_Data(
           j,(mid2+ceil(Correction_r(j))))−Error_Data(j,(mid2+floor(
           Correction_r(j)))));
        Theta_r_mod(j,1) = Error_Data(j,(mid2+floor(Correction_r(j)))
           )+adder;

    else
        Theta_r_mod(j,1) = Error_Data(j,(mid2+Correction_r(j)));

    end


    if Correction_l(j) == 0
        Theta_l_mod(j,1) = Theta_l(j);

    elseif round(Correction_l(j)) ≠ Correction_l(j)


        adder = (Correction_l(j)−floor(Correction_l(j)))*(Error_Data(
           j,(mid1+ceil(Correction_l(j))))−Error_Data(j,(mid1+floor(
           Correction_l(j)))));
        Theta_l_mod(j,1) = Error_Data(j,(mid1+floor(Correction_l(j)))
           )+adder;
    else
        Theta_l_mod(j,1) = Error_Data(j,(mid1+Correction_l(j)));

    end
end



Final_Data = cat(2,Vol,Theta_l,Theta_r,Theta_l_mod,Theta_r_mod);
save([filepath,'Final_data.mat'],'Final_Data')

%%
figure
plot(Vol,Theta_l_mod,'ro',Vol,Theta_r_mod,'bo')

% eof
```

REFERENCES

James Larminie and Andrew Dicks. *Fuel Cells Systems Explained.* John Wiley & Sons Ltd,, 2003.

Jeffrey S. Allen. An analytical solution for determination of small contact angles from sessile drops of arbitrary size. *Journal of Colloid and Interface Science*, 261(2):481 – 489, 2003. ISSN 0021-9797.

A.F. Stalder, G. Kulik, D. Sage, L. Barbieri, and P. Hoffmann. A snake-based approach to accurate determination of both contact points and contact angles. *Colloids and Surfaces A: Physicochemical and Engineering Aspects*, 286(1-3):92 – 103, 2006. ISSN 0927-7757.

F. Bashforth and J.C. Adams. *An Attempt to Test the Theories of Capillary Action by Comparing the theoretical and Measured Forms of Drops of Fluid-Liquid.* Cambride University Press, London, 1883.

Stanley Hartland and Richard W. Hartley. *Axisymmetric Fluid-Liquid Interfaces.* Elsevier, 1976.

P. Cheng, D. Li, L. Boruvka, Y. Rotenberg, and A.W. Neumann. Automation of axisymmetric drop shape analysis for measurements of interfacial tensions and contact angles. *Colloids and Surfaces*, 43(2):151 – 167, 1990. ISSN 0166-6622. Selected Papers from a Symposium on Recent Progress in Interfacial Tensiometry, held at the Third Chemical Congress of North America.

Robert N. Wenzel. Resistance of solid surfaces to wetting by water. *Industrial & Engineering Chemistry*, 28(8):988–994, August 1936. ISSN 0019-7866.

A. B. D. Cassie and S. Baxter. Wettability of porous surfaces. *Trans. Faraday Soc.*, 40:546–551, 1944. ISSN 0014-7672.

Jaroslaw Drelich and Jan D. Miller. Modification of the cassie equation. *Langmuir*, 9(2):619–621, February 1993. ISSN 0743-7463.

Russell Stacey. Contact angle measurement technique for rough surfaces. Master's thesis, Michigan Technological University, 2009.

A. W. Neumann and Jan K. Spelt, editors. *Applied Science Thermodynamics*. Marcel Dekker, Inc., 1996.

J. D. Miller, S. Veeramasuneni, J. Drelich, M. R. Yalamanchili, and G. Yamauchi. Effect of roughness as determined by atomic force microscopy on the wetting properties of ptfe thin films. *Polym Eng Sci*, 36(14):1849–1855, 1996. ISSN 1548-2634.

S. Veeramasuneni, J. Drelich, J. D. Miller, and G. Yamauchi. Hydrophobicity of ion-plated ptfe coatings. *Progress in Organic Coatings*, 31(3):265 – 270, 1997. ISSN 0300-9440.

Bo He, Junghoon Lee, and Neelesh A. Patankar. Contact angle hysteresis on rough hydrophobic surfaces. *Colloids and Surfaces A: Physicochemical and Engineering Aspects*, 248(1-3):101 – 104, 2004. ISSN 0927-7757.

Abraham Marmur. The lotus effect: Superhydrophobicity and metastability. *Langmuir*, 20(9):3517–3519, April 2004. ISSN 0743-7463.